Article

Neuron

A Common Neuroendocrine Substrate for Diverse General Anesthetics and Sleep

Highlights

- General-anesthesia-activated neurons (AANs) are identified in hypothalamus
- AANs consist mainly of neuroendocrine cells in and near the supraoptic nucleus
- Activation of AANs promotes slow-wave sleep and extends general anesthesia
- Inhibition of AANs shortens general anesthesia and disrupts natural sleep

Authors

Li-Feng Jiang-Xie, Luping Yin, Shengli Zhao, Vincent Prevosto, Bao-Xia Han, Kafui Dzirasa, Fan Wang

Correspondence

fan.wang@duke.edu

In Brief

Jiang-Xie et al. identified a specific group of hypothalamic neurons (AANs) commonly activated by multiple classes of general anesthetics. Stimulation of AANs potentiates slow-wave sleep and general anesthesia (GA), whereas inhibition of AANs disrupts natural sleep and destabilizes GA.

Jiang-Xie et al., 2019, Neuron *102*, 1053–1065
June 5, 2019
https://doi.org/10.1016/j.neuron.2019.03.033

CellPress

Neuron
Article

A Common Neuroendocrine Substrate for Diverse General Anesthetics and Sleep

Li-Feng Jiang-Xie,[1,4] Luping Yin,[1,4] Shengli Zhao,[1] Vincent Prevosto,[1,2] Bao-Xia Han,[1] Kafui Dzirasa,[1,3] and Fan Wang[1,5,*]
[1]Department of Neurobiology, Duke University Medical Center, Durham, NC 27710, USA
[2]Department of Biomedical Engineering, Duke University, Durham, NC 27710, USA
[3]Department of Psychiatry and Behavioral Sciences, Duke University Medical Center, Durham, NC 27710, USA
[4]These authors contributed equally
[5]Lead Contact
*Correspondence: fan.wang@duke.edu
https://doi.org/10.1016/j.neuron.2019.03.033

SUMMARY

How general anesthesia (GA) induces loss of consciousness remains unclear, and whether diverse anesthetic drugs and sleep share a common neural pathway is unknown. Previous studies have revealed that many GA drugs inhibit neural activity through targeting GABA receptors. Here, using Fos staining, *ex vivo* brain slice recording, and *in vivo* multichannel electrophysiology, we discovered a core ensemble of hypothalamic neurons in and near the supraoptic nucleus, consisting primarily of neuroendocrine cells, which are persistently and commonly activated by multiple classes of GA drugs. Remarkably, chemogenetic or brief optogenetic activations of these anesthesia-activated neurons (AANs) strongly promote slow-wave sleep and potentiates GA, whereas conditional ablation or inhibition of AANs led to diminished slow-wave oscillation, significant loss of sleep, and shortened durations of GA. These findings identify a common neural substrate underlying diverse GA drugs and natural sleep and reveal a crucial role of the neuroendocrine system in regulating global brain states.

INTRODUCTION

The discovery of general anesthetics has revolutionized surgical procedures in medicine over the past centuries (Franks, 2008; Robinson and Toledo, 2012). Each year, millions of patients worldwide undergo general anesthesia (GA) for medical treatments. GA is a global brain and body state characterized by unconsciousness, analgesia, amnesia, and immobility while maintaining vital physiological functions (Brown et al., 2010; Franks, 2008). Despite decades of scientific effort, the target and circuit mechanisms by which extremely diverse groups of GA drugs all can induce sedation and loss of consciousness remain poorly understood (Alkire et al., 2008; Brown et al., 2010; Franks, 2008; Koch et al., 2016; Rudolph and Antkowiak, 2004). Delineating the identities of neurons and the precise neural circuitry that enable GA drugs to produce the unconscious brain state will advance our basic understandings and clinical applications of GA.

During the past decades, GABA (γ-aminobutyric acid) type A ($GABA_A$) receptor has emerged as a principal target for many anesthetics (Franks, 2008). $GABA_A$ receptor is the major contributor of neuronal inhibition and widely expressed throughout the CNS. Many GA drugs have been shown to potentiate GABA-induced Cl^- current; in higher doses, they can directly activate $GABA_A$ receptors (Franks, 2008). On the other hand, there are also non-GABAergic anesthetics, such as ketamine, which targets the NMDA receptor to reduce the excitatory action of glutamate, and dexmedetomidine, which binds to alpha-2 (α2) adrenergic receptors and inhibits the norepinephrine release from locus coeruleus (Franks, 2008). Together, these results lead to the idea that different GA drugs work by exerting differentiated inhibitory impacts on the nervous system, although the particular loci (if present) that anesthetics target to induce unconsciousness is still elusive. In recent years, a few studies have identified anesthetic-activated cells in several brain regions, using either immediate early gene markers or *ex vivo* brain slice recording (Gelegen et al., 2018; Moore et al., 2012; Zhang et al., 2015a). However, no study so far has provided conclusive evidence of anesthetic-activated neurons with *in vivo* electrophysiology, and whether there is a common neural substrate activated by different classes of GA drugs is unknown.

The overlap between GA and endogenous sleep-wake circuitry is also actively debated. Examination of brain oscillations revealed that, although different anesthetics produce distinct patterns of electroencephalography (EEG) that may not be observed in natural sleep, one of the shared features of sleep and GA is the enhancement of slow-delta (0.5–4 Hz) oscillations (Akeju and Brown, 2017; Franks, 2008; Rudolph and Antkowiak, 2004). Notably, sleep deprivation results in increased homeostatic pressure to sleep and enhances the potency of GA (Tung et al., 2002). The recovery process from sleep deprivation can also take place during GA (Tung et al., 2004). However, the exact biological substrate shared between GA and sleep remains to be identified. In recent years, a few studies have revealed that neurons' co-release of peptides and small molecule transmitters (glutamate or GABA) participate in regulating sleep across different species (Chung et al., 2017; Jego et al., 2013; Lee et al., 2017). Compared to fast transmitters, neuropeptides exert

wider spreading and longer-lasting effects, which are ideally suited to regulate global brain state. However, the potential roles of neuropeptides in GA are largely an uncharted territory, and whether there are common neuropeptides engaged in both sleep and GA is unexplored.

Here, we reasoned that neurons activated by multiple different GA drugs may represent a shared substrate between GA and sleep. Using a combination of immediate early gene expression, *ex vivo* brain slice, and *in vivo* extracellular recordings, we uncovered a hypothalamic neuronal population, which unexpectedly consists primarily of neuroendocrine cells that are surprisingly and persistently activated by multiple distinct GA drugs. With our recently developed capturing activated neuronal ensembles (CANE) technology (Sakurai et al., 2016), we were able to precisely label, characterize, and manipulate these anesthesia-activated neurons (AANs). In freely behaving mice, optogenetic and chemogenetic activation of AANs were sufficient to strongly potentiate slow-wave sleep (SWS) and GA. Importantly, conditional ablation of AANs resulted in significant decline of slow-wave power and loss of both SWS and REM (rapid eye movement) sleep, and acute inhibition of AANs shortened the duration of GA. Together, our results revealed a previously unrecognized critical function of neuroendocrine cells, which are known for their role of releasing hormones, in regulating both GA and natural sleep.

RESULTS

Discovery of AANs *In Vivo*

Initially, to search for AANs, we subjected the mice to either isoflurane-oxygen anesthesia or to oxygen exposure alone (control) for 2 h, followed by examining the brain for Fos expression. Fos is an immediate early gene that is generally used as a marker for activated neurons (Morgan and Curran, 1989). As compared to control condition, Fos expression throughout the brain was dramatically diminished under isoflurane GA, and we observed a distinct cluster of strong Fos^+ neurons in the ventral region of the hypothalamus (Figure 1A), a region containing neurons regulating sleep-wake cycles (Scammell et al., 2017; Weber and Dan, 2016). Notably, most of the AANs (>80% of Fos^+ cells) resided at the upper corner of the optic chiasm, extending through the anterior-to-posterior axis of the ventral edge of the hypothalamus, which is classically defined as the supraoptic nucleus (SON) (Figure 1A), located posterior to the ventrolateral preoptic nucleus (VLPO) (Kroeger et al., 2018). There was also a sparse population of AANs scattered from ventral preoptic area (POA) to areas dorsal to posterior SON under isoflurane (Figure 1A); we refer to these regions collectively as the *para*SON area.

Although Fos is considered as a neuronal activity marker, other cellular events (such as signaling of neurotrophic factors or activation of protein kinase A) might induce Fos expression without neuronal firing (Lin et al., 2008). To gain more direct evidence that AAN indeed increases firing *in vivo* under GA, we recorded well-isolated single-unit activity in AAN region with simultaneous monitoring of local field potentials (LFPs) in frontal cortex and electromyography (EMG) in neck muscle (as indicators of brain states) before, during, and after GA (Dzirasa et al., 2011; Figures 1B–1G and S1; n = 89 neurons from 7 mice). We classified the identified single units into three categories based on their responsiveness toward isoflurane exposure. Although the majority of recorded cells were either suppressed (36%) or weakly modulated (53%) by isoflurane, a small population of neurons (11%; 10 out of 89) with low baseline activity was strongly and persistently activated under GA (Figures 1C, 1D, and 1G). Importantly, a significant portion of these activated cells (60%; 6 of these 10) increased firing rates before the brain state transitioned from wakefulness to the loss of consciousness state (LOC) as determined by the LFP and EMG recording (Figures 1E and S2), and the majority of cells (70%; 7 of the 10) decreased firing before the animal emerged from GA (Figures 1F and S2). These results suggested that GA indeed elicits robust and persistent firing of AANs *in vivo*.

Molecular Signatures of AANs

We next characterized the neurochemical signatures of AANs. Previous research had suggested that GA drugs and SWS activated hypothalamic GABAergic and/or galaninergic neurons in POA (Moore et al., 2012; Sherin et al., 1998). On the other hand, SON is known to contain peptidergic neuroendocrine cells that mainly produce arginine vasopressin (AVP) (also known as antidiuretic hormone [ADH]), prodynorphin (Pdyn), or oxytocin (OXT) (Ludwig and Leng, 2006; Mutsuga et al., 2004). Using two-color *in situ* hybridization, in which AANs were identified with *Fos* RNA probe (induced by isoflurane GA), we found that 45.20% scattered AANs in the paraSON region were $vGat^+$, and 44.67% were $vGlut2^+$ (Figure 2). Thus, the paraSON AANs contained both inhibitory and excitatory cells. However, AANs located within SON were largely but weakly $vGlut2^+$ (Ponzio et al., 2006; 95.39%). Further investigation revealed around 80% AANs in SON expressed *AVP* and *Pdyn* (85.95% for *AVP*; 81.22% for *Pdyn*), and 10.87% SON AANs were $Galanin^+$ (Figure 2). AANs were largely non-overlapping with the high-level (bright) *OXT*-expressing SON cells. However, under GA, there appeared a population of low (dim) level of oxytocin expression SON cells that was not present in control (un-anesthetized) conditions (Figure S3A). Interestingly, 89.26% AANs showed dim *OXT* expression (Figure 2). It has been known that SON AVP cells express very low level of oxytocin in basal condition (Leng, 2018). These results suggest that GA may induce *OXT* mRNA expression in AANs. Overall, the hypothalamic AAN population is largely composed of peptidergic neurons (which are also weakly $vGlut2^+$) in SON and sparsely distributed GABAergic and glutamatergic cells in paraSON.

AANs Represent a Common Substrate Targeted by Multiple Distinct GA Drugs

To further characterize and manipulate AANs, we employed the recently developed capturing activated neuronal ensemble (CANE) technology (Sakurai et al., 2016), which is ideally suited to express any desired transgene in Fos^+ neurons (Figure 3A). This CANE system utilizes engineered pseudotyped lentivirus (CANE-LV) that selectively infects Fos^+ neurons in the Fos^{TVA} knockin mice. We subjected Fos^{TVA} mice to 2 h isoflurane GA, followed by co-injection of CANE-LV-Cre with Cre-dependent

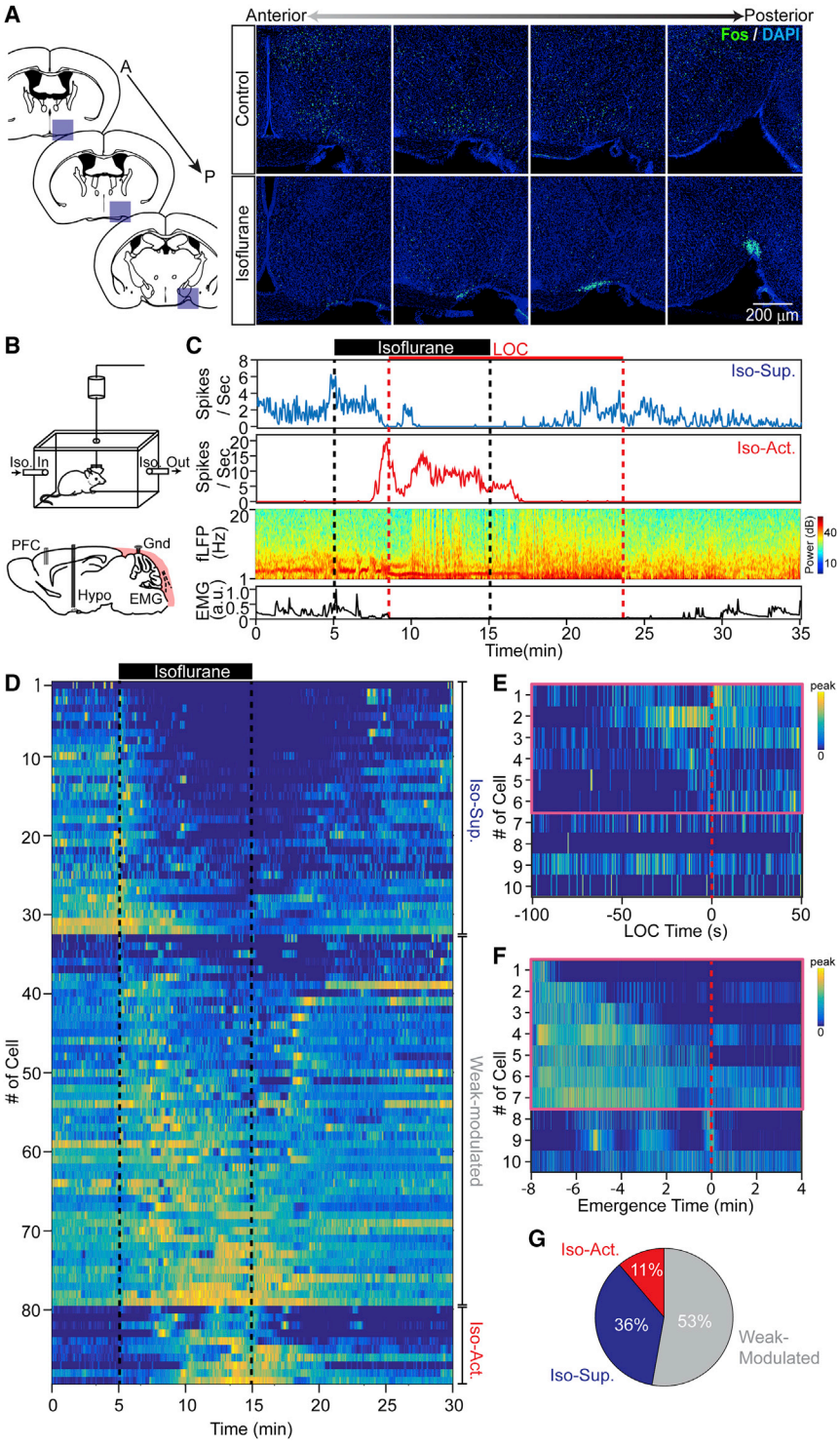

Figure 1. Discovery of AANs in Hypothalamus

(A) (Left) Schematics of interested regions on the brain atlas. A, anterior; P, posterior. (Right) Representative patterns of Fos$^+$ neurons (approximately 0 mm to −1.2 mm from bregma) after 2-h control (oxygen) versus isoflurane exposure (1%∼1.2% isoflurane mixed with oxygen) from n = 4 pairs of mice are shown.

(B–G) Simultaneous *in vivo* extracellular recording of hypothalamic neurons in the AAN region and the brain states before, during, and after GA. n = 89 neurons across 14 sessions from 7 mice.

(B) Schematics of recording chamber and electrode placement. EMG, electromyography; Gnd, ground; Iso, isoflurane; PFC, prefrontal cortex.

(C) Representative isoflurane-suppressed (Iso-Sup.) and isoflurane-activated (Iso-Act.) neuron. (Top two) Spike rate of the example neuron, (third) frontal cortex LFP (fLFP), and (bottom) EMG are shown. Black dashed lines mark the duration of isoflurane exposure. Red dashed lines indicate the period of loss of consciousness (LOC).

(D) Activity profile of all neurons recorded (n = 89). The spike rate of each neuron was normalized by its peak firing rate.

(E and F) Activities of isoflurane-activated neurons (raw spike trains convolved with 1 s Gaussian kernel) aligned with the time when mice lose consciousness (E) or emerge from GA (F). Purple square highlights the neurons that increased firing rate before LOC (E) or decreased firing rate ahead of emergence (F).

(G) Categorize the neuronal population based on its response toward isoflurane.

See also Figures S1 and S2.

AAV-DIO-mCherry into AAN region (Figure 3B). 3∼4 weeks later, the mice were re-exposed to 2 h of isoflurane GA, and the activated neurons were visualized with Fos staining. We found that 92.72% of CANE-mCherry-labeled neurons in SON and 73.87% in paraSON re-expressed Fos$^+$ after second isoflurane GA, suggesting that the same ensemble of AANs was re-activated by the repeated GA (Figures 3C and 3D).

The CANE capturing of AANs also afforded us the opportunity to examine whether isoflurane-activated AANs can also be activated by other GA drugs. To do this, we first used CANE to express mCherry in isoflurane-activated AANs, and weeks later, we subjected the mice to treatment of either propofol, ketamine (with or without xylazine), or dexmedetomidine (Dex), followed by Fos staining (Franks, 2008; Figures 3D and S3B). Interestingly, propofol, ketamine (plus xylazine), and Dex all re-activated a large population of AANs that were previously activated by isoflurane in both SON and paraSON (Figure 3D). In SON, 76.64%, 97.85%, and 75.98% isoflurane-mCherry$^+$ cells were Fos$^+$ under propofol, ketamine, and Dex, respectively; in paraSON, 56.32%, 70.28%, and 65.45% isoflurane-mCherry$^+$ cells were Fos$^+$ under propofol, ketamine (plus xylazine), and Dex, respectively. Ketamine alone also re-activated a shared population of AANs, albeit

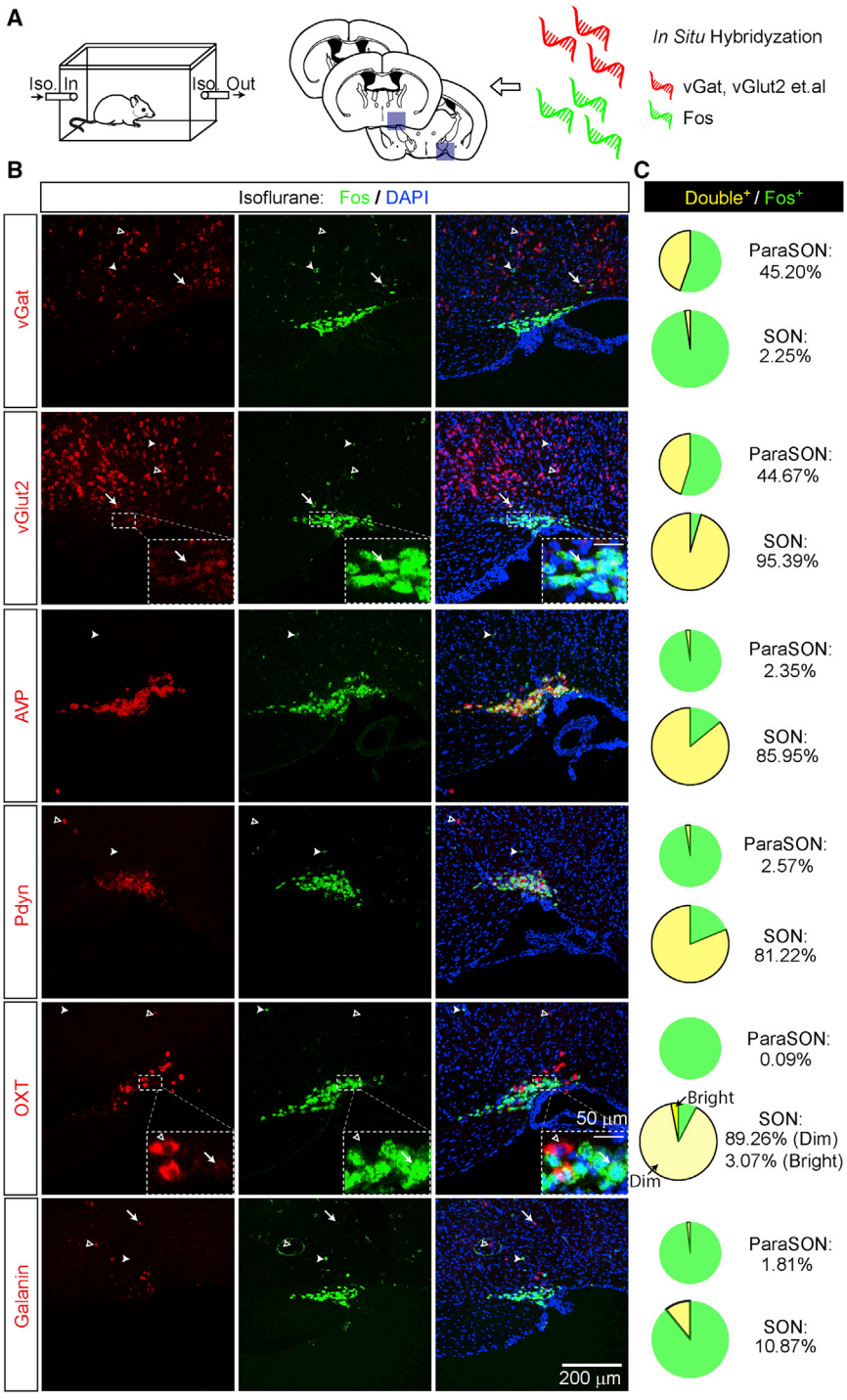

Figure 2. Molecular Signatures of AAN

(A) Experimental procedure of two-color *in situ* hybridization on AANs. vGat, vesicular GABA transporter; vGlut2, vesicular glutamate transporter 2; AVP, arginine vasopressin; OXT, oxytocin; Pdyn, prodynorphin.

(B) Representative images of two-color *in situ* hybridization between Fos (green) that marks AANs and following probes (red): vGat; vGlut2; AVP; Pdyn; OXT; and Galanin. Arrow, open arrowhead, and solid arrowhead indicating double$^+$, probe$^+$ only, and Fos$^+$ only cells, respectively, are shown.

(C) Pie chart of percentage of AANs (Fos$^+$) colocalized with each probe in SON and paraSON region. Neurons were from 7–23 sections from 2 or 3 mice for each pair of conditions.

See also Figure S3.

to a lesser extent (Figure S3B). We further performed whole-cell patch-clamp recording of CANE-mCherry captured AANs (mostly in SON). We discovered that isoflurane, propofol, ketamine, and Dex all significantly depolarized the membrane potentials of AANs upon perfusion into the acute brain slices (Figure 3E; $\Delta V = 11.38 \pm 1.82$ mV induced by isoflurane, n = 11; $\Delta V = 5.10 \pm 0.98$ mV induced by propofol, n = 32; $\Delta V = 7.09 \pm 1.89$ mV induced by ketamine, n = 25; $\Delta V = 12.95 \pm 1.79$ mV induced by Dex, n = 27 recorded AAN), consistent with the fact that these cells became Fos$^+$ *in vivo* under GA. Together, our results strongly support the idea that these hypothalamic AANs represent a common neural substrate activated by distinct classes of GA drugs.

Chemogenetic Activation of AANs Strongly Enhances SWS

We next wanted to determine the causal functions by artificially activating AANs. Because the entire population of AANs (SON plus paraSON) is distributed from ventral preoptic regions to the most posterior end of SON (>1.2 mm along the anterior-posterior axis in the ventral hypothalamus), we exploited chemogenetics (Roth, 2016) to activate this spatially extended population of neurons. The chemogenetic activator hM3Dq-DREADDs (AAN-hM3Dq) or control mCherry (AAN-mCherry) was expressed in AANs using CANE (Figures 4A–4C). In acute brain slices, application of clozapine-n-oxide (CNO), the ligand for hM3Dq, resulted in persistent firing of hM3Dq-expressing AANs (Figure 4C). Systemic injection of CNO also induced robust Fos expression in AAN-hM3Dq mice (Figure 4B). To examine the *in vivo* effects on brain states, we injected AAN-hM3Dq or control AAN-mCherry mice with either CNO or saline and simultaneously recorded the EEG from frontal and parietal cortex and EMG from the neck muscle for 2 h immediately after injection (during dark phase; Figure 4A). In saline-injected AAN-hM3Dq, as well as saline- or CNO-injected AAN-mCherry control mice, we observed normal interspersed wakefulness and short bouts

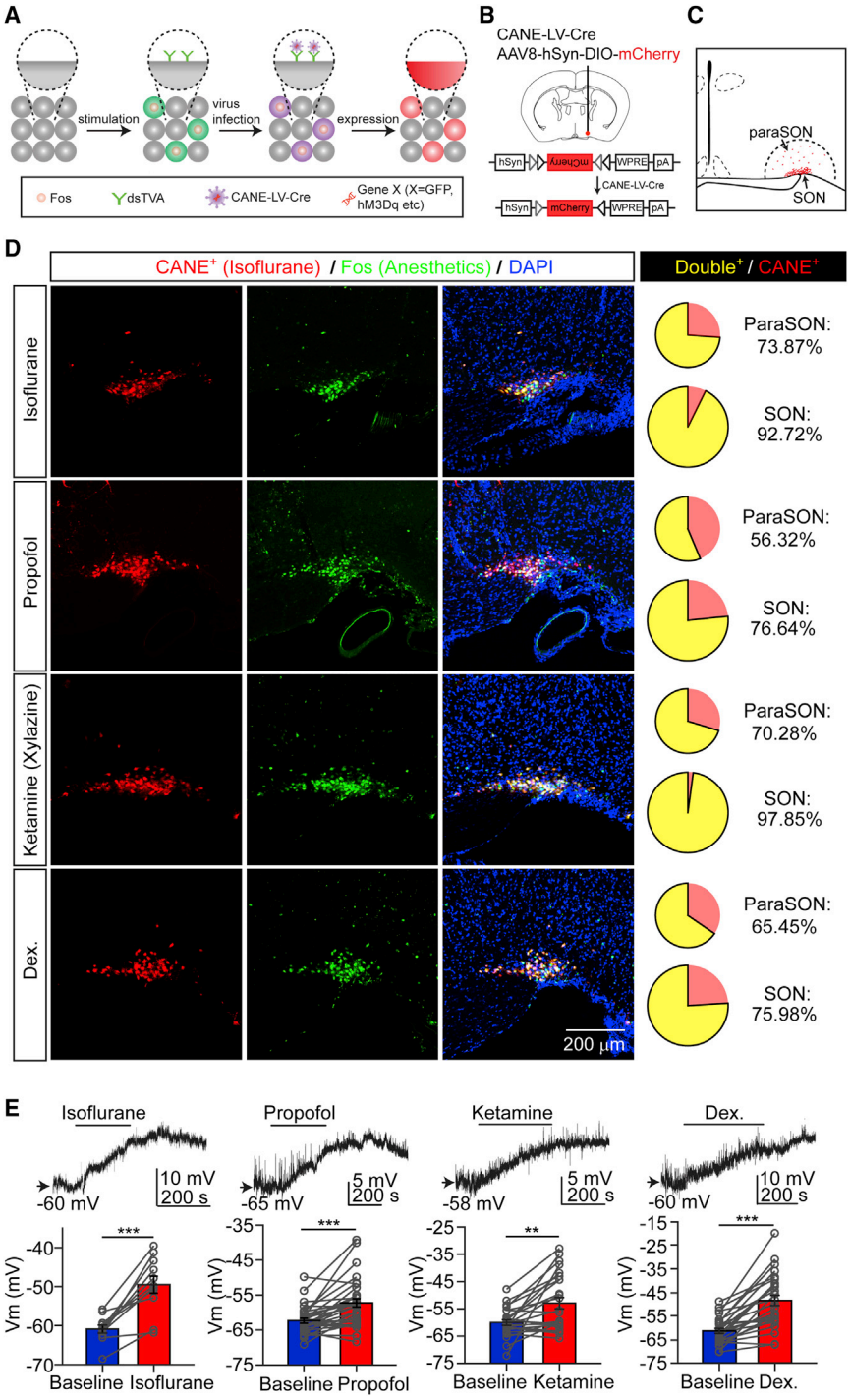

Figure 3. A Shared Neuronal Population Is Activated by Different Anesthetics

(A) Schematic diagram of CANE technology.

(B) Viral construct and injection site in Fos^{TVA} mice.

(C) Illustration of the SON and paraSON. paraSON is defined as a region within 500 μm radius circle with the up-corner of the optic chiasm or tract as the center, extending from anterior to posterior hypothalamus.

(D) (Left) Representative images of CANE-captured isoflurane-activated neurons (red) and Fos$^+$ neurons (green) induced by re-exposure to either isoflurane again or to propofol, ketamine (plus xylazine), or dexmedetomidine (Dex). (Right) Pie charts showing the percentage of initial CANE-captured, isoflurane-activated neurons that are re-activated (Fos$^+$) by different anesthetics in SON as well as in paraSON. Neurons were from 7–30 slices from 2–4 mice for each condition.

(E) Whole-cell patch-clamp recording of CANE-captured isoflurane-activated neurons in acute brain slices following treatments of different classes of anesthetics. (Top) Representative membrane potential changes after the application of drugs are shown; (bottom) statistical summary for all recorded neurons is shown. n = 11 neurons for isoflurane; n = 32 for propofol; n = 25 for ketamine; n = 27 for Dex. Wilcoxon signed-rank tests for all drugs are shown.

Data are presented as mean ± SEM. $^{**}p < 0.01$; $^{***}p < 0.001$.

See also Figure S3.

of SWS characterized by higher power oscillations at delta (1–4 Hz) frequency and low EMG activity and occasional episodes of REM sleep characterized by elevated theta oscillation with very low amplitude of EMG (Scammell et al., 2017; Weber and Dan, 2016; Figures 4D and 4E). Remarkably, in CNO-treated AAN-hM3Dq mice, the average total duration of SWS nearly doubled that of three control groups, and the average total wake period was concomitantly reduced (Figures 4D and 4E; on average, 56.53% ± 3.70% of time SWS for hM3Dq-CNO versus 28.30% ± 2.71%, 23.86% ± 2.36%, and 24.83% ± 1.05% for hM3Dq-saline, mCherry-saline, and mCherry-CNO conditions, respectively). This SWS-enhancing effect of chemogenetic activation of AANs was primarily attributable to extending the average SWS bout duration (Figure 4F; average 48.01 ± 4.85 s per SWS bout for hM3Dq-CNO versus 26.95 ± 3.50, 24.52 ± 3.10, and 27.35 ± 3.26 s for hM3Dq-saline, mCherry-saline, and mCherry-CNO conditions, respectively, during dark phase with 4-s scoring window). In other words, activating AANs renders mice asleep much longer but does not alter their sleep frequency. We further performed detailed spectral analyses on frontal and parietal EEGs. The power-frequency curves of SWS under AAN activation almost completely overlapped with those of the naturally occurring SWS with the peak power at delta wave both in frontal and parietal EEG (Figures 4G, 4H, and S4). Taken together, our results strongly suggest that AANs identified here likely represent the shared neural pathway between different GA drugs

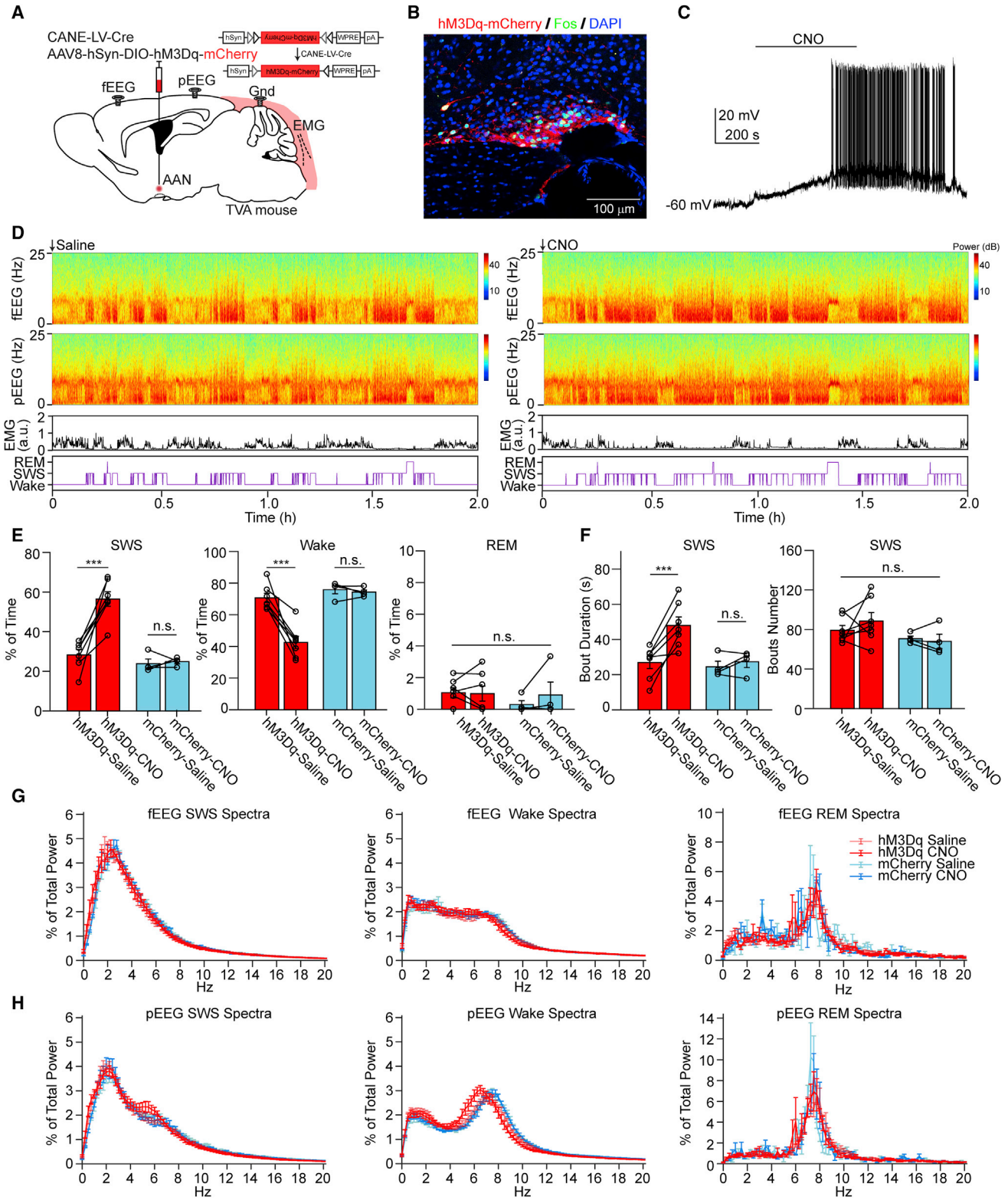

Figure 4. Chemogenetic Activation of AAN Significantly Potentiates SWS

(A) Viral-genetic strategy for expressing hM3Dq-mCherry in AANs, and the layout of EEG and EMG recording. fEEG, frontal EEG; Gnd, ground; pEEG, parietal EEG.

(B) Systemic CNO treatment (intraperitoneal injection) induced robust Fos (green) expression in the hM3Dq-mCherry^{+} (red) neurons.

(legend continued on next page)

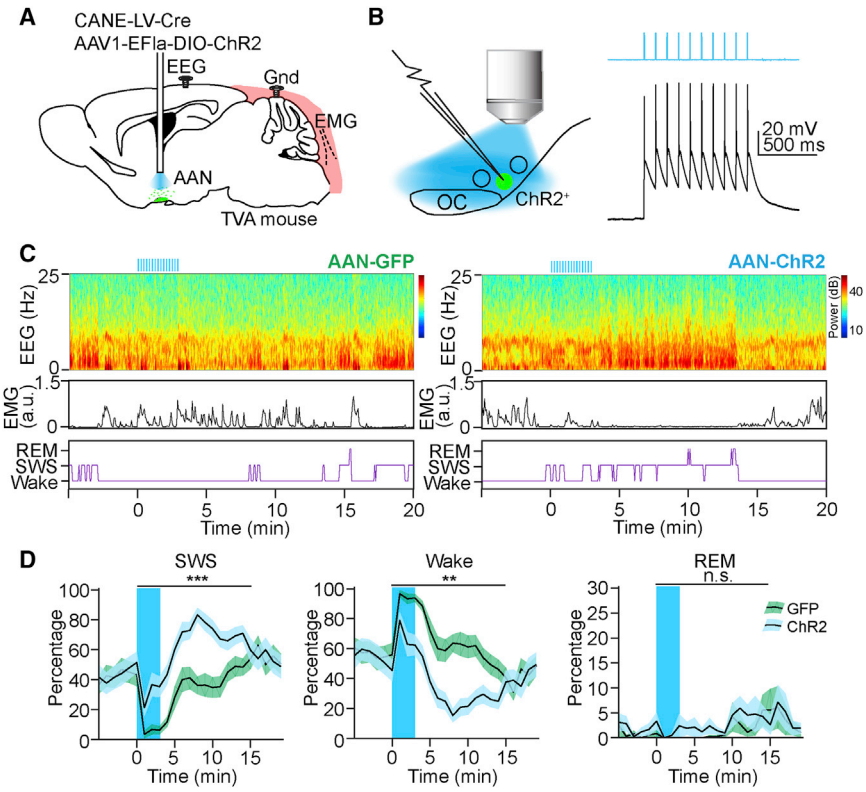

Figure 5. Brief Optogenetic Activation of AAN Promotes Subsequent SWS

(A) Viral-genetic strategy for expressing ChR2 in AANs, the layout of optic fiber implantation, and EEG and EMG recording.

(B) Blue laser evokes reliable neuronal spikes in ChR2^{+} AANs.

(C) Representative polysomnographic recording of AAN-GFP (left) and AAN-ChR2 (right) mice before, during, and after laser stimulation (10 Hz; 10-ms pulses; 1 s-ON and 1 s-OFF; 3 min; 3∼4 mW measured at the fiber tips). (Top) Representative spectrogram of EEG, (middle) EMG, and (bottom) brain state annotated are shown.

(D) Percentage of time spent in SWS (left), wake (middle), and REM (right) before, during, and after the period of laser stimulation (blue shaded area). n = 28 trials from 5 ChR2 mice (4∼6 trials per mouse); n = 24 trials from 4 GFP mice (6 trials per mouse). Permutation test was performed across two groups.

Data are presented as mean ± SEM. $^{**}p < 0.01$; $^{***}p < 0.001$.

See also Figure S6.

and natural sleep and that activating AANs is sufficient to promote and extend the duration of SWS.

Because the majority of cells among AANs were previously unsuspected SON neurons, which were validated as neuroendocrine cells using the classical Fluorogold uptake assay (Figure S3C; Weiss and Cobbett, 1992), we next asked whether activating the specific SON cells alone is sufficient to increase SWS. Although there is no available Cre-driver line that expresses in all SON-AAN, we decided to utilize AVP$^{Cre/+}$ mice because ∼85% of SON-AANs are *AVP*$^{+}$ cells (which also co-express *Pdyn*; Watson et al., 1982), keeping in mind the caveat that AVP^{Cre} mice are homozygous lethal (our observation). We injected Cre-dependent AAV-DIO-hM3Dq bilaterally into SON of heterozygous AVP$^{Cre/+}$ mice and implanted EEG and EMG electrodes in the same mice. Chemogenetic activation of SON AVP^{+} neurons alone was indeed sufficient to potentiate SWS (Figure S5; 27.74% ± 1.89% and 46.87% ± 2.11% of time spent in SWS for saline and CNO conditions), although the extent of SWS duration increase was less than that induced by activating all AAN (99.75% SWS increase for activating all AAN versus 68.96% for activating SON AVP^{+} neurons). Our results thus reveal a previously under-appreciated role of vasopressin^{+}/dynorphin^{+} SON neuroendocrine cells in promoting SWS.

Brief Optogenetic Activation of AANs Promotes Subsequent Sleep and Potentiates GA

AANs include a large proportion of neuroendocrine cells, which are able to secrete large quantities of peptides into the cerebrospinal fluid through somatodendritic release (Ludwig and Leng, 2006). Considering that peptide signaling generally lasts longer than classic neurotransmitters, we therefore asked whether a brief stimulation of AANs is sufficient to promote and sustain subsequent sleep. To this end, we expressed the light-activated cation channel channelrhodopsin 2 (AAN-ChR2) (Boyden et al., 2005; Yizhar et al., 2011) or control GFP (AAN-GFP) in AANs using CANE, followed by implantation of fiber optics (200 μm) bilaterally above the AANs (Figure 5A). We validated that blue light (10 Hz; 10 ms) indeed drove robust neuronal firing of labeled AANs in acute brain slices (Figure 5B). We first performed

(C) Depolarization of hM3Dq-mCherry^{+} neurons by CNO in acute brain slice.

(D) Representative polysomnographic recording following either saline or CNO treatment in AAN-hM3Dq mouse. (Top two) Representative spectrogram from fEEG and pEEG, (third) EMG, and (bottom) brain state annotated are shown. REM, rapid-eye movement sleep; SWS, slow-wave sleep.

(E) Percentage of time spent in SWS, wake, and REM across 2 h after injection. Two-way repeated-measures ANOVA followed by Sidak's post hoc test is shown. n = 7 mice for hM3Dq-mCherry and n = 4 mice for mCherry group.

(F) Bout duration and number of SWS across 2 h after injection. Two-way repeated-measures ANOVA followed by Sidak's post hoc test is shown. n = 7 mice for hM3Dq and n = 4 mice for mCherry group.

(G and H) Power-frequency analysis of fEEG (G) and pEEG (H) across SWS, wake, and REM from different experimental groups is shown. n = 7 mice for hM3Dq and n = 4 mice for mCherry group.

Data are presented as mean ± SEM. $^{***}p < 0.001$.

See also Figures S4 and S5.

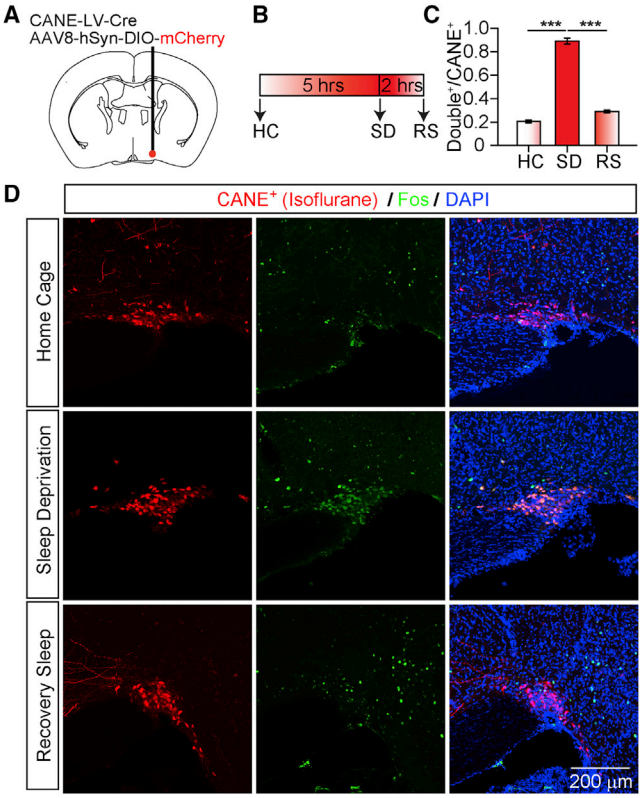

Figure 6. AAN Is Activated by Sleep Pressure

(A) CANE strategy for specifically expressing mCherry in AAN.

(B) Time windows for each experimental group. HC, home cage; RS, recovery sleep; SD, sleep deprivation.

(C) Total percentage of CANE-captured neurons re-activated under HC, SD, and RS. One-way ANOVA followed by Sidak's post hoc test is shown. n = 3 mice for HC, n = 4 for SD, and n = 3 for RS.

(D) Representative Fos staining from HC, SD, and RS.

Data are presented as mean ± SEM. ***p < 0.001.

photo-stimulation in control AAN-GFP mice. To our surprise, we discovered that laser stimulation (10 Hz, 10 ms/pulse, and 1 s ON and 1 s OFF, for total of 3 min) had a significant arousal effect on control AAN-GFP animals during the stimulation period (Figures 5C and 5D). Because the fibers were implanted closely above AANs, which are located immediately dorsal to optic chiasm, we reasoned that such deep brain photo-illumination might activate melanopsin-expressing retinal ganglion cells and promote wakefulness. Indeed, a previous study demonstrated that optogenetic deep brain stimulation resulted in retinal activation (Danskin et al., 2015). Remarkably, despite the artifact of light-induced arousal, the same 3 min of laser stimulation in AAN-ChR2 mice drastically increased SWS in the post-stimulation period, signified by a dominant delta oscillation (1–4 Hz) and minimal muscle activity. More interestingly, the sleep-promoting effect lasted up to 10 min after the laser was turned off (Figures 5C and 5D), indicating that a brief activation of AANs is sufficient to exert a long-lasting effect on brain state. We also observed a complementary decrease in wake time, and there was no significant difference in REM during the post-stimulation period in AAN-ChR2 mice (Figures 5C and 5D). The optogenetic effect of AANs on SWS also prompted us to investigate the consequence of activating AANs on subsequent GA induction and emergence. Isoflurane (1%) was infused immediately after photo-stimulation (10 Hz, 10 ms/pulse, and 1 s ON and 1 s OFF, for total of 3 min), and the brain states of animals were determined by EEG and EMG recording. Interestingly, we discovered that photo-activation of AANs did not alter the GA induction but significantly delayed the emergence from GA. In other words, animals would stay longer under GA once we activated AANs (Figure S6), again consistent with the idea of long-lasting peptidergic signaling in sustaining a global sedative state.

AAN Is Activated by Sleep Pressure

We next investigated the relationship between AAN activity and natural sleep. AANs were first labeled with mCherry using CANE in a cohort of mice (Figure 6A). Subsequently, these mice were randomly assigned into three groups: (1) staying in home cage without any disturbance; (2) undergoing sleep deprivation for 5 h; and (3) undergoing sleep deprivation for 5 h followed by recovery sleep for 2 h. Afterward, their brains were collected for Fos staining (Figure 6B). Interestingly, we discovered that sleep deprivation strongly activated AAN. After recovery sleep, the Fos expression in AAN gradually returned to baseline (Figures 6C and 6D). These results suggest that it is the need for sleep (sleep pressure) that drives the activation of these neurons. This finding also dovetails nicely with our optogenetic experiment result in that activation of AAN can promote subsequent SWS.

Ablation of AAN Disrupts Natural Sleep

Although AAN activation is sufficient to promote SWS, we wanted to know whether AANs are necessary for naturally occurring sleep. To test this, we expressed either the diphtheria toxin receptor (DTR) (AAN-DTR) (Saito et al., 2001) or control mCherry (AAN-mCherry) in AANs using CANE (Figures 7A and S7). We performed chronic EEG and EMG recordings (whole day) before and after diphtheria toxin (DT) injection induced ablation of AANs that expressed DTR (Figure 7B). In AAN-DTR mice, over the course of 2 weeks post-DT injection, the total duration of both SWS and REM sleep gradually and significantly declined (Figures 7C and 7D; n = 9 mice, SWS: 39.09% ± 0.97%, 38.34% ± 1.23%, 37.69% ± 1.94%, 26.55% ± 2.30%, and 22.42% ± 3.19% of time; REM: 5.46% ± 0.41%, 5.62% ± 0.43%, 2.60% ± 0.43%, 1.59% ± 0.39%, and 1.85% ± 0.49% of time at baseline, day 2, 5, 1 week, or 2 weeks post-DT, respectively). Interestingly, the effect on SWS is largely due to shortened bout duration (but not the total bout numbers), indicating ablating AANs caused the inability to sustain SWS (Figure 7E; average SWS bout duration: 100.23 ± 7.82, 83.24 ± 5.75, 77.34 ± 7.20, 56.93 ± 8.28, and 43.94 ± 6.33 s at baseline, day 2, 5, 1 week, or 2 weeks post-DT, respectively, averaged across the whole day recording with 10-s scoring window). On the other hand, the reduction in REM sleep is mainly attributable to reduced bout numbers (but not per bout duration), suggesting that the AAN-DTR mice had a difficulty in entering REM sleep (Figure 7F; average REM bout number: 86.89 ± 4.97, 102.00 ± 9.16, 42.56 ± 9.83, 26.56 ± 6.88, and 32.11 ± 8.57 number of bouts at baseline, day 2, 5, 1 week, or 2 weeks post-DT, respectively). Moreover, we noticed that the

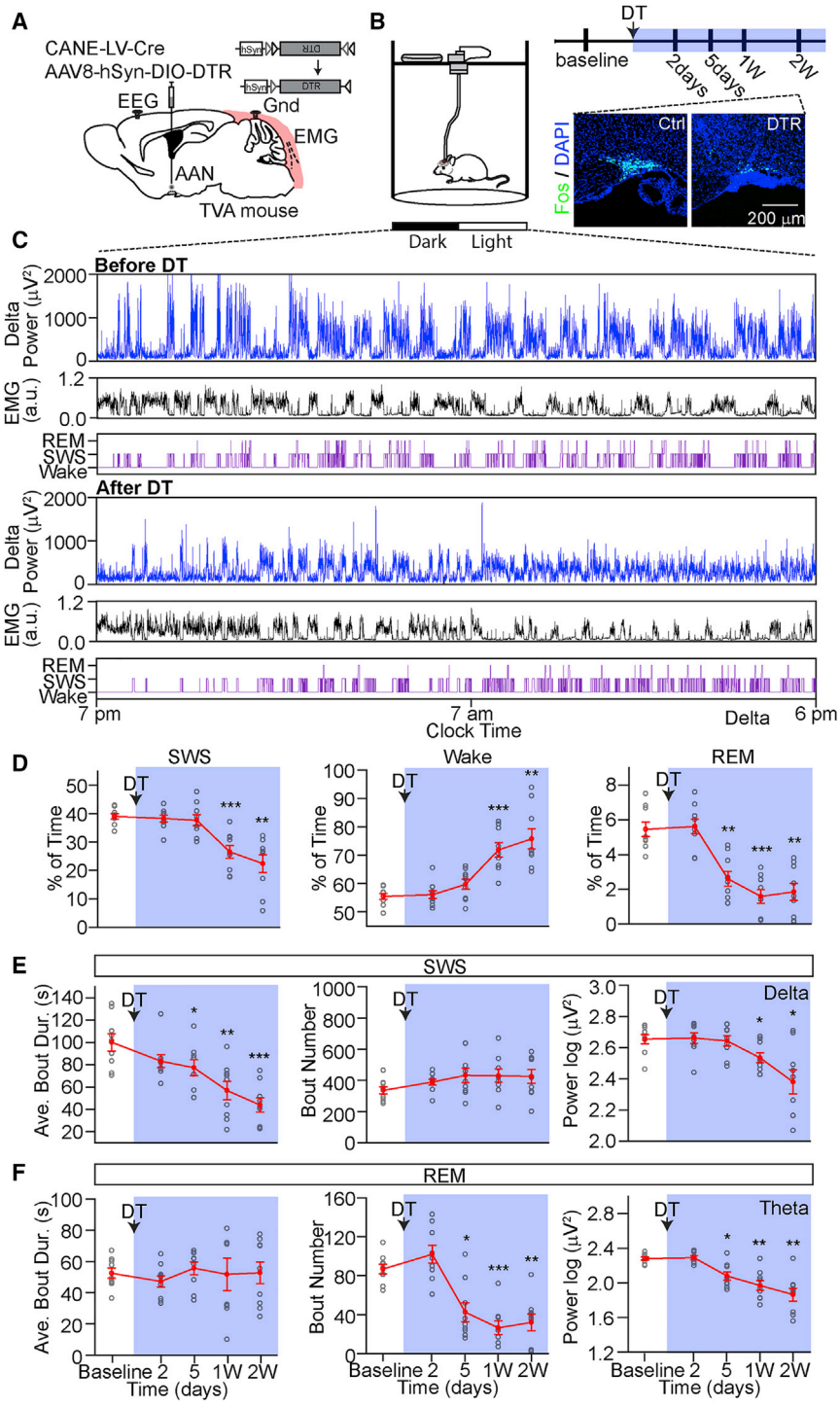

Figure 7. Ablation of AAN Disrupts Natural Sleep

(A) (Left) Viral-genetic strategy for specifically expressing diphtheria toxin receptor (DTR) in AANs and the layout of EEG and EMG electrodes.

(B) (Left) Experimental setup of EEG and EMG recording across day and night. (Right, top) Experimental design and the timing of DT injection are shown. (Right, bottom) Representative image of AAN ablation after DT injection is shown. DT, diphtheria toxin; 1W, 1 week after DT; 2W, 2 weeks after DT.

(C) Representative polysomnographic recording before (top) and after (bottom) DT treatment in AAN-DTR mice.

(D) Total percentage of time spent in SWS (left), wake (middle), and REM (right) across 23 h recording. One-way repeated-measures ANOVA followed by Sidak's post hoc test is shown. n = 9 mice.

(E) Average bout duration, bout number, and delta power of SWS. One-way repeated-measures ANOVA followed by Sidak's post hoc test is shown. n = 9 mice.

(F) Average bout duration, bout number, and theta power of REM sleep. One-way repeated-measures ANOVA followed by Sidak's post hoc test is shown. n = 9 mice.

Data are presented as mean ± SEM. *p < 0.05; **p < 0.01; ***p < 0.001.

See also Figure S7.

delta power of SWS and the theta power of REM sleep were gradually declined in AAN-DTR mice, suggesting that neuronal oscillations, which are signatures of normal sleep, were impaired (Figures 7E and 7F, right-most panels). One-third of animals (3 out of 9 mice) eventually died at the end of experimental session (~3 weeks), presumably due to severe sleep deprivation. Importantly, none of these effects were observed in DT-treated AAN-mCherry mice (Figure S7). Together, our results indicated that AANs are essential for promoting and stabilizing natural sleep.

Optogenetic Inhibition of AAN Shortens the Duration of GA

We had wanted to determine whether ablation of AANs could affect GA induction or duration. However, DTR-mediated killing of AANs led to either mortality or chronic sleep loss, which are known to confound GA assay. We therefore turned to perform acute silencing of AANs with optogenetics. We expressed the light-activated proton pump (AAN-eArch3.0; Chow et al., 2010) or control GFP (AAN-GFP) in AANs using CANE, followed by implantation of fiber optics (200 μm) bilaterally above the AANs (Figure 8A). We validated that yellow light indeed induced sustained hyperpolarization of AANs expressing proton pump eArch3.0 (Figure 8B). For *in vivo* experiments, isoflurane (1%) was co-administered with yellow light (5 min square pulse), and the brain states of animals were monitored by EEG and EMG. Inhibition of AAN did not alter GA induction but significantly shortened the duration of GA (Figures 8C–8F). These

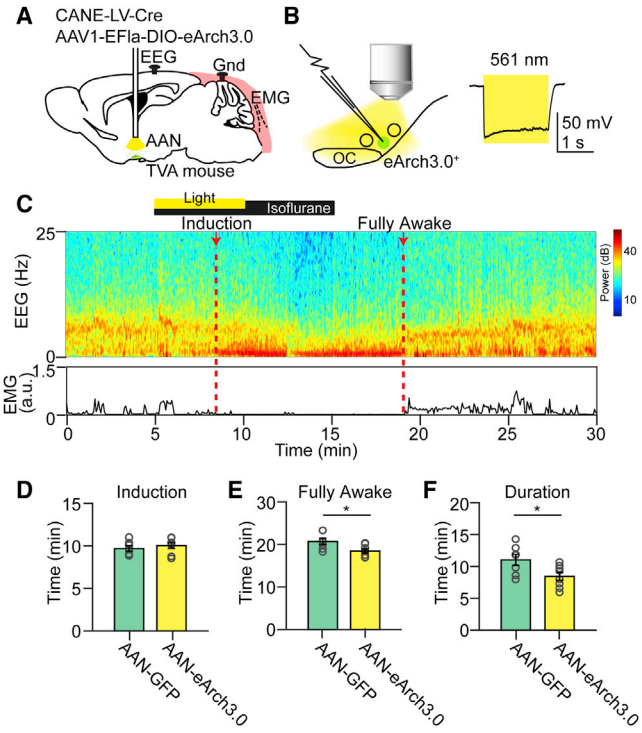

Figure 8. Optogenetic Inhibition of AAN Shortens the Duration of GA

(A) Viral-genetic strategy for expressing eArch3.0 in AANs, the layout of optic fiber implantation, and EEG and EMG recording.

(B) Yellow light induces a sustained hyperpolarization in eArch3.0$^+$ AANs.

(C) Representative EEG and EMG recording across experimental session. (Top) Spectrogram of EEG is shown; (bottom) EMG is shown. Isoflurane (1%) was infused for 10 min. Yellow laser stimulation (5-min square pulse; 5∼7 mW measured at the fiber tips) was applied for the first 5 min of isoflurane infusion. Induction time is identified by occurrence of slow oscillation and reduction of movement. Fully awake time is determined by reduction in slow wave power and raised muscle activity continuously for more than 1 min.

(D–F) Statistical analysis of induction time (D), fully awake time (E), and anesthesia duration (F). n = 7 for AAN-GFP mice; n = 8 for AAN-eArch3.0 mice. Two-sample t test is shown.

Data are presented as mean ± SEM. *p < 0.05.

results further underscore the importance of the slow but long-lasting peptidergic (hormonal) signaling in maintaining the GA state.

Downstream Targets of AAN

Finally, we asked in addition to the pituitary gland, a well-known axonal target of peptidergic SON neurons, whether AANs have any other downstream structure inside the brain. We used CANE technology to express GFP in AANs and mapped their projections throughout the whole mouse brain (Figure S8). We found that AANs project to the septum, a structure known to pace the theta wave (6–10 Hz) of the hippocampus (Buzsáki, 2002) and to the anterior thalamus, a brain region critical for modulating slow-wave activity in EEG (David et al., 2013). We also observed AAN axons in several brain areas engaged in arousal control, including posterior lateral hypothalamus (PLH) (Yamashita and Yamanaka, 2017), tuberomammillary nucleus (TMN) (Yu et al., 2015), supramammillary nucleus (MM) (Pedersen et al., 2017), lateral habenula (LHb) (Gelegen et al., 2018), periaqueductal gray (PAG) (Weber et al., 2018), ventral tegmental area (VTA) (Eban-Rothschild et al., 2016; Taylor et al., 2016), median raphe nucleus (MnR), pedunculopontine nucleus (PPTg), as well as laterodorsal tegmental nucleus (LDTg) (Van Dort et al., 2015). It is interesting to note that LHb is one of AAN targets. A recent study discovered that activities of LHb excitatory neurons are required for natural sleep as well as for propofol-induced sedation (Gelegen et al., 2018). Finally, as expected, a large axon bundle was observed that travels toward the arcuate nucleus and median eminence (ARC-ME), which is the known axon pathway for SON axons *en route* to the posterior pituitary, where hormones are released to the general circulation.

DISCUSSION

The conventional view on GA drugs' mode of action is that they generally inhibit neuronal activities. Here, we demonstrate that chemically distinct GA drugs (isoflurane, propofol, ketamine, and dexmedetomidine) all activate a common hypothalamic neural ensemble (AAN) composed mainly of peptidergic (AVP/Pdyn/Galanin) neuroendocrine cells in SON (Figure 2), as evidenced both in slice preparations and *in vivo* measurements (Figures 1 and 3). Optogenetic and chemogenetic activation of these AANs was sufficient to promote SWS and potentiate GA (Figures 4, 5, and S5), whereas ablating these AANs led to reduced slow-wave power, sleep fragmentation (reduced SWS bout duration), and loss of total sleep (both SWS and REM; Figure 7). Furthermore, acute silencing of AANs with optogenetics shortened the duration of GA (Figure 8). Together, these results identify a common neural substrate at the intersection of sleep and GA.

In recent years, a couple of studies have identified AANs in several brain regions, using either Fos labeling or brain slice recording (Gelegen et al., 2018; Lu et al., 2008; Moore et al., 2012; Zhang et al., 2015a). Here, we were able to unequivocally demonstrate the presence of AANs *in vivo* through multi-channel recordings and simultaneous brain state monitoring (Figures 1C and 1D). Importantly, leveraging the fine temporal resolution afforded by electrophysiology, we found that theses AANs could fire persistently during GA and even ahead of the time when animals lose consciousness (Figure 1E). In addition, the AANs discovered in this study can be activated by multiple classes of anesthetics (Figure 3), although the underlying mechanisms of depolarization will require further investigation. Interestingly, a recent study showed that GABA is excitatory in adult SON AVP cells due to intracellular Cl^- accumulation (Haam et al., 2012). Because a large number of anesthetics target GABA receptors, we speculate SON AANs could be depolarized by other anesthetics as well. On the other hand, several studies discovered that a wide variety of general anesthetics (including halothane, isoflurane, sevoflurane, propofol, ketamine, and dexmedetomidine) could directly interact with G-protein-coupled receptors (GPCRs) (Ho et al., 2015; Minami and Uezono, 2013). Because the downstream signaling pathway of excitatory GPCRs can increase intracellular calcium release from stores, which in turn can facilitate neuropeptides and hormones release, we speculate that GA drugs may activate some GPCRs in AANs to produce depolarization.

Perhaps the most surprising finding is that the majority of AANs are peptidergic neuroendocrine cells located in SON (vasopressin$^+$, dynorphin$^+$, and galanin$^+$ neurons; Figure 2). Magnocellular SON neurons combine the properties of classical neurons and canonical endocrine cells (Leng, 2018; Figure S3C). Their axons travel all the way to the pituitary gland, and their dendrites cover major areas of the posterior hypothalamus. As neurons, they generate action potentials to trigger hormone release from the pituitary gland into general circulation; as endocrine cells, they directly release peptides from their dendrites and somas in large amount. Within the cerebrospinal fluid, the concentration of peptides detected is high enough to activate targeted receptors in distant brain regions (Ludwig and Leng, 2006). Thus, neuroendocrine cells are ideally positioned to jointly regulate both brain and body state.

Our results indicate that AANs express numerous peptides, mainly AVP, Pdyn, and galanin (Figure 2). Interestingly, these neuropeptides have been implicated in the sleep process. The secretion of SON AVP was previously found to typically increase during the hours of sleep both in human and rodents (Forsling, 1993; Trudel and Bourque, 2010), and enhanced AVP release was implicated in preventing dehydration (Trudel and Bourque, 2010) and lowering body temperature (Hicks et al., 2014) during sleep. AVP also regulates the water channel *aquaporin-4*, which is highly expressed in astrocytes and is a key component of the glymphatic system that has been implicated in driving metabolism clearance during sleep (Niermann et al., 2001; Xie et al., 2013). Dynorphin (encoded by *Pdyn* gene), when infused into hypothalamus, has the potential to drastically increase the duration of SWS (Greco et al., 2008). Galanin and its homolog have been shown to promote sleep in several species (Chen et al., 2017; Donlea et al., 2018; Kroeger et al., 2018). Thus, these peptides could potentially regulate multiple aspects of brain and body physiology required for promoting and sustaining sleep. A recent sequencing effort has identified SON as one of the most genetically heterogeneous tissues in the body (Mure et al., 2018); thus, other as yet unidentified neuropeptides might participate in promoting sleep. On the other hand, AANs also express vGlut2 (albeit at low levels), and glutamate released by these cells could play a role in promoting sleep through activating downstream targets, a possibility awaiting future investigations.

In addition to their activation by multiple general anesthetics (Figure 3), we showed that AANs also respond to sleep pressure (Figure 6). Previous studies had demonstrated that endogenous somnogen prostaglandin D2 (PGD_2) and interleukin-6 could strongly activate SON neurons (Palin et al., 2009; Scammell et al., 1998). Utilizing amino-cupric-silver staining, a previous study also revealed that SON is the most affected region in prolonged sleep deprivation (Eiland et al., 2002). Thus, SON AAN might not be activated by sleep itself but by the drive to sleep. In addition, SON has been shown to highly express prostaglandin-H2 D-isomerase (PTGDS) (Mure et al., 2018), which converts prostaglandin H2 to PGD_2, and secrete the precursor of adenosine, ATP (Brown et al., 2008). Both PGD_2 and adenosine are elevated in sleep-deprived animals, and intracerebroventricular infusion of these molecules potentiates SWS (Bjorness and Greene, 2009; Urade and Hayaishi, 2011). This is also consistent with our finding that a brief optogenetic stimulation of AAN is sufficient to strongly promote SWS in post-stimulation period (Figure 5). More than a century ago, it was found that the cerebrospinal fluid of sleep-deprived animals could promote sleep in other animals (Kubota, 1989). It is conceivable that sleep pressure induced AANs to release peptides and other small molecules into cerebrospinal fluid. Because the receptors for these molecules are widely expressed in the brain, they can influence brain-wide neural activities and work on a longer timescale than classic neurotransmitters, thereby globally coordinating the brain to enter into the sleep and unconscious state.

In fact, activation of AANs by sleep drive instead of sleep per se would be in accordance with other innate homeostatic systems, such as feeding and drinking. The neurons that promote feeding (Agrp$^+$ cells in ARC) and drinking (Nos$^+$ cells in the subfornical organ) are not activated by eating or drinking itself but by the desire to eat (hunger) or drink (thirst). Their activity actually decreases immediately after a source of food or water appears (Betley et al., 2015; Zimmerman et al., 2017). Homeostatic regulation of sleep-wake behavior may thus follow the same logic. Future investigation is needed to carefully determine whether SON AANs play a critical role in homeostatic regulation of sleep and to determine which peptides or small molecules the SON AANs release into the brain (or body) once being activated by sleep pressure. Taken together, our results reveal a common and previously unknown neuroendocrine substrate that is targeted by multiple classes of anesthetic drugs and is also required for natural sleep. These results also bring the neuroendocrine system to the forefront of both practice and future research in GA and sleep medicine.

STAR★METHODS

Detailed methods are provided in the online version of this paper and include the following:

- KEY RESOURCES TABLE
- CONTACT FOR REAGENT AND RESOURCE SHARING
- EXPERIMENTAL MODEL AND SUBJECT DETAILS
  - Animals
- METHOD DETAILS
  - Viral Vectors
  - Immunofluorescence
  - Two-Color *in situ* Hybridization
  - Capturing AANs Using CANE
  - Labeling of Neuroendocrine Cells with Peripheral Fluorogold Injection
  - Axon-Tracing and Quantification
  - Multi-channel *In Vivo* Recording and Data Analysis
  - Slice Electrophysiology
  - Drug Administration
  - EEG and EMG Recording and Analysis
  - Mild Sleep Deprivation and Recovery
- QUANTIFICATION AND STATISTICAL ANALYSIS
- DATA AND SOFTWARE AVAILABILITY

SUPPLEMENTAL INFORMATION

Supplemental Information can be found online at https://doi.org/10.1016/j.neuron.2019.03.033.

A video abstract is available at https://doi.org/10.1016/j.neuron.2019.03.033#mmc3.

ACKNOWLEDGMENTS

We thank Drs. Richard Mooney, Stephen Lisberger, Nicolas Brunel, and the members of the Wang lab for discussion and critical reading of the manuscript. We thank Stephen Mague for the training of animal surgery and electrode construction. We thank Gary Lehew for providing the circuit board design in electrophysiology recording. We thank Zhigang He and Chen Wang for providing AAV-DIO-DTR. We thank Dr. Max Kelz for guidance of recording isoflurane responsiveness in brain slices. We thank Satya Achanta for help with some experiments using propofol. This work is supported by NIH DP1MH103908 to F.W., a Brain Research Foundation SIA to F.W., a W.M. Keck Foundation grant to F.W. and K.D., and the Human Frontier Science Program (LT000038/2018-L) to L.Y.

AUTHOR CONTRIBUTIONS

F.W. and L.-F.J.-X. conceived the original idea. F.W., L.-F.J.-X., and L.Y. designed the experiments. L.-F.J.-X. performed the multi-channel *in vivo* extracellular recording. K.D. provided the training and advices on extracellular recording. L.Y. performed the slice electrophysiology. L.-F.J.-X. and L.Y. performed the activation and ablation experiments with EEG and EMG recordings. L.Y., L.-F.J.-X., and S.Z. performed the Fos staining and *in situ* hybridization. L.-F.J.-X. and L.Y. analyzed the data. V.P. gave advice on the data analysis. S.Z. generated CANE viruses for this study. B.-X.H. handled the mouse colony and genotyping and bred all mice for this study. L.-F.J.-X., L.Y., V.P., K.D., and F.W. wrote the manuscript.

DECLARATION OF INTERESTS

The authors declare no competing interests.

Received: November 14, 2018
Revised: February 12, 2019
Accepted: March 20, 2019
Published: April 18, 2019

REFERENCES

Akeju, O., and Brown, E.N. (2017). Neural oscillations demonstrate that general anesthesia and sedative states are neurophysiologically distinct from sleep. Curr. Opin. Neurobiol. *44*, 178–185.

Alkire, M.T., Hudetz, A.G., and Tononi, G. (2008). Consciousness and anesthesia. Science *322*, 876–880.

Bellavance, M.A., Takatoh, J., Lu, J., Demers, M., Kleinfeld, D., Wang, F., and Deschênes, M. (2017). Parallel inhibitory and excitatory trigemino-facial feedback circuitry for reflexive vibrissa movement. Neuron *95*, 722–723.

Betley, J.N., Xu, S., Cao, Z.F.H., Gong, R., Magnus, C.J., Yu, Y., and Sternson, S.M. (2015). Neurons for hunger and thirst transmit a negative-valence teaching signal. Nature *521*, 180–185.

Bjorness, T.E., and Greene, R.W. (2009). Adenosine and sleep. Curr. Neuropharmacol. *7*, 238–245.

Boyden, E.S., Zhang, F., Bamberg, E., Nagel, G., and Deisseroth, K. (2005). Millisecond-timescale, genetically targeted optical control of neural activity. Nat. Neurosci. *8*, 1263–1268.

Brown, C.H., Ruan, M., Scott, V., Tobin, V.A., and Ludwig, M. (2008). Multifactorial somato-dendritic regulation of phasic spike discharge in vasopressin neurons. Prog. Brain Res. *170*, 219–228.

Brown, E.N., Lydic, R., and Schiff, N.D. (2010). General anesthesia, sleep, and coma. N. Engl. J. Med. *363*, 2638–2650.

Buzsáki, G. (2002). Theta oscillations in the hippocampus. Neuron *33*, 325–340.

Chen, S., Reichert, S., Singh, C., Oikonomou, G., Rihel, J., and Prober, D.A. (2017). Light-dependent regulation of sleep and wake states by prokineticin 2 in zebrafish. Neuron *95*, 153–168.e6.

Chow, B.Y., Han, X., Dobry, A.S., Qian, X., Chuong, A.S., Li, M., Henninger, M.A., Belfort, G.M., Lin, Y., Monahan, P.E., and Boyden, E.S. (2010). High-performance genetically targetable optical neural silencing by light-driven proton pumps. Nature *463*, 98–102.

Chung, S., Weber, F., Zhong, P., Tan, C.L., Nguyen, T.N., Beier, K.T., Hörmann, N., Chang, W.C., Zhang, Z., Do, J.P., et al. (2017). Identification of preoptic sleep neurons using retrograde labelling and gene profiling. Nature *545*, 477–481.

Danskin, B., Denman, D., Valley, M., Ollerenshaw, D., Williams, D., Groblewski, P., Reid, C., Olsen, S., Blanche, T., and Waters, J. (2015). Optogenetics in mice performing a visual discrimination task: measurement and suppression of retinal activation and the resulting behavioral artifact. PLoS ONE *10*, e0144760.

David, F., Schmiedt, J.T., Taylor, H.L., Orban, G., Di Giovanni, G., Uebele, V.N., Renger, J.J., Lambert, R.C., Leresche, N., and Crunelli, V. (2013). Essential thalamic contribution to slow waves of natural sleep. J. Neurosci. *33*, 19599–19610.

Donlea, J.M., Pimentel, D., Talbot, C.B., Kempf, A., Omoto, J.J., Hartenstein, V., and Miesenböck, G. (2018). Recurrent circuitry for balancing sleep need and sleep. Neuron *97*, 378–389.e4.

Dzirasa, K., Fuentes, R., Kumar, S., Potes, J.M., and Nicolelis, M.A. (2011). Chronic in vivo multi-circuit neurophysiological recordings in mice. J. Neurosci. Methods *195*, 36–46.

Eban-Rothschild, A., Rothschild, G., Giardino, W.J., Jones, J.R., and de Lecea, L. (2016). VTA dopaminergic neurons regulate ethologically relevant sleep-wake behaviors. Nat. Neurosci. *19*, 1356–1366.

Eiland, M.M., Ramanathan, L., Gulyani, S., Gilliland, M., Bergmann, B.M., Rechtschaffen, A., and Siegel, J.M. (2002). Increases in amino-cupric-silver staining of the supraoptic nucleus after sleep deprivation. Brain Res. *945*, 1–8.

Forsling, M.L. (1993). Neurohypophysial hormones and circadian rhythm. Ann. N Y Acad. Sci. *689*, 382–395.

Franks, N.P. (2008). General anaesthesia: from molecular targets to neuronal pathways of sleep and arousal. Nat. Rev. Neurosci. *9*, 370–386.

Gelegen, C., Miracca, G., Ran, M.Z., Harding, E.C., Ye, Z., Yu, X., Tossell, K., Houston, C.M., Yustos, R., Hawkins, E.D., et al. (2018). Excitatory pathways from the lateral habenula enable propofol-induced sedation. Curr. Biol. *28*, 580–587.e5.

Greco, M.A., Fuller, P.M., Jhou, T.C., Martin-Schild, S., Zadina, J.E., Hu, Z., Shiromani, P., and Lu, J. (2008). Opioidergic projections to sleep-active neurons in the ventrolateral preoptic nucleus. Brain Res. *1245*, 96–107.

Haam, J., Popescu, I.R., Morton, L.A., Halmos, K.C., Teruyama, R., Ueta, Y., and Tasker, J.G. (2012). GABA is excitatory in adult vasopressinergic neuroendocrine cells. J. Neurosci. *32*, 572–582.

Hicks, C., Ramos, L., Reekie, T., Misagh, G.H., Narlawar, R., Kassiou, M., and McGregor, I.S. (2014). Body temperature and cardiac changes induced by peripherally administered oxytocin, vasopressin and the non-peptide oxytocin receptor agonist WAY 267,464: a biotelemetry study in rats. Br. J. Pharmacol. *171*, 2868–2887.

Ho, J., Perez-Aguilar, J.M., Gao, L., Saven, J.G., Matsunami, H., and Eckenhoff, R.G. (2015). Molecular recognition of ketamine by a subset of olfactory G protein-coupled receptors. Sci. Signal. *8*, ra33.

Jego, S., Glasgow, S.D., Herrera, C.G., Ekstrand, M., Reed, S.J., Boyce, R., Friedman, J., Burdakov, D., and Adamantidis, A.R. (2013). Optogenetic identification of a rapid eye movement sleep modulatory circuit in the hypothalamus. Nat. Neurosci. *16*, 1637–1643.

Koch, C., Massimini, M., Boly, M., and Tononi, G. (2016). Neural correlates of consciousness: progress and problems. Nat. Rev. Neurosci. *17*, 307–321.

Kriegsfeld, L.J., Korets, R., and Silver, R. (2003). Expression of the circadian clock gene Period 1 in neuroendocrine cells: an investigation using mice with a Per1:GFP transgene. Eur. J. Neurosci. *17*, 212–220.

Kroeger, D., Absi, G., Gagliardi, C., Bandaru, S.S., Madara, J.C., Ferrari, L.L., Arrigoni, E., Münzberg, H., Scammell, T.E., Saper, C.B., and Vetrivelan, R.

(2018). Galanin neurons in the ventrolateral preoptic area promote sleep and heat loss in mice. Nat. Commun. *9*, 4129.

Kubota, K. (1989). Kuniomi Ishimori and the first discovery of sleep-inducing substances in the brain. Neurosci. Res. *6*, 497–518.

Lee, D.A., Andreev, A., Truong, T.V., Chen, A., Hill, A.J., Oikonomou, G., Pham, U., Hong, Y.K., Tran, S., Glass, L., et al. (2017). Genetic and neuronal regulation of sleep by neuropeptide VF. eLife *6*, e25727.

Leng, G. (2018). The Heart of the Brain: The Hypothalamus and Its Hormones (The MIT Press).

Lin, Y., Bloodgood, B.L., Hauser, J.L., Lapan, A.D., Koon, A.C., Kim, T.K., Hu, L.S., Malik, A.N., and Greenberg, M.E. (2008). Activity-dependent regulation of inhibitory synapse development by Npas4. Nature *455*, 1198–1204.

Lu, J., Nelson, L.E., Franks, N., Maze, M., Chamberlin, N.L., and Saper, C.B. (2008). Role of endogenous sleep-wake and analgesic systems in anesthesia. J. Comp. Neurol. *508*, 648–662.

Ludwig, M., and Leng, G. (2006). Dendritic peptide release and peptide-dependent behaviours. Nat. Rev. Neurosci. *7*, 126–136.

Minami, K., and Uezono, Y. (2013). The recent progress in research on effects of anesthetics and analgesics on G protein-coupled receptors. J. Anesth. *27*, 284–292.

Moore, J.T., Chen, J., Han, B., Meng, Q.C., Veasey, S.C., Beck, S.G., and Kelz, M.B. (2012). Direct activation of sleep-promoting VLPO neurons by volatile anesthetics contributes to anesthetic hypnosis. Curr. Biol. *22*, 2008–2016.

Morgan, J.I., and Curran, T. (1989). Stimulus-transcription coupling in neurons: role of cellular immediate-early genes. Trends Neurosci. *12*, 459–462.

Mure, L.S., Le, H.D., Benegiamo, G., Chang, M.W., Rios, L., Jillani, N., Ngotho, M., Kariuki, T., Dkhissi-Benyahya, O., Cooper, H.M., and Panda, S. (2018). Diurnal transcriptome atlas of a primate across major neural and peripheral tissues. Science *359*, eaao0318.

Mutsuga, N., Shahar, T., Verbalis, J.G., Brownstein, M.J., Xiang, C.C., Bonner, R.F., and Gainer, H. (2004). Selective gene expression in magnocellular neurons in rat supraoptic nucleus. J. Neurosci. *24*, 7174–7185.

Niermann, H., Amiry-Moghaddam, M., Holthoff, K., Witte, O.W., and Ottersen, O.P. (2001). A novel role of vasopressin in the brain: modulation of activity-dependent water flux in the neocortex. J. Neurosci. *21*, 3045–3051.

Oh, S.W., Harris, J.A., Ng, L., Winslow, B., Cain, N., Mihalas, S., Wang, Q., Lau, C., Kuan, L., Henry, A.M., et al. (2014). A mesoscale connectome of the mouse brain. Nature *508*, 207–214.

Oyola, M.G., Thompson, M.K., Handa, A.Z., and Handa, R.J. (2017). Distribution and chemical composition of estrogen receptor β neurons in the paraventricular nucleus of the female and male mouse hypothalamus. J. Comp. Neurol. *525*, 3666–3682.

Palin, K., Moreau, M.L., Sauvant, J., Orcel, H., Nadjar, A., Duvoid-Guillou, A., Dudit, J., Rabié, A., and Moos, F. (2009). Interleukin-6 activates arginine vasopressin neurons in the supraoptic nucleus during immune challenge in rats. Am. J. Physiol. Endocrinol. Metab. *296*, E1289–E1299.

Pedersen, N.P., Ferrari, L., Venner, A., Wang, J.L., Abbott, S.B.G., Vujovic, N., Arrigoni, E., Saper, C.B., and Fuller, P.M. (2017). Supramammillary glutamate neurons are a key node of the arousal system. Nat. Commun. *8*, 1405.

Ponzio, T.A., Ni, Y., Montana, V., Parpura, V., and Hatton, G.I. (2006). Vesicular glutamate transporter expression in supraoptic neurones suggests a glutamatergic phenotype. J. Neuroendocrinol. *18*, 253–265.

Prerau, M.J., Brown, R.E., Bianchi, M.T., Ellenbogen, J.M., and Purdon, P.L. (2017). Sleep neurophysiological dynamics through the lens of multitaper spectral analysis. Physiology (Bethesda) *32*, 60–92.

Robinson, D.H., and Toledo, A.H. (2012). Historical development of modern anesthesia. J. Invest. Surg. *25*, 141–149.

Roth, B.L. (2016). DREADDs for neuroscientists. Neuron *89*, 683–694.

Rudolph, U., and Antkowiak, B. (2004). Molecular and neuronal substrates for general anaesthetics. Nat. Rev. Neurosci. *5*, 709–720.

Saito, M., Iwawaki, T., Taya, C., Yonekawa, H., Noda, M., Inui, Y., Mekada, E., Kimata, Y., Tsuru, A., and Kohno, K. (2001). Diphtheria toxin receptor-mediated conditional and targeted cell ablation in transgenic mice. Nat. Biotechnol. *19*, 746–750.

Sakurai, K., Zhao, S., Takatoh, J., Rodriguez, E., Lu, J., Leavitt, A.D., Fu, M., Han, B.X., and Wang, F. (2016). Capturing and manipulating activated neuronal ensembles with CANE delineates a hypothalamic social-fear circuit. Neuron *92*, 739–753.

Scammell, T., Gerashchenko, D., Urade, Y., Onoe, H., Saper, C., and Hayaishi, O. (1998). Activation of ventrolateral preoptic neurons by the somnogen prostaglandin D2. Proc. Natl. Acad. Sci. USA *95*, 7754–7759.

Scammell, T.E., Arrigoni, E., and Lipton, J.O. (2017). Neural circuitry of wakefulness and sleep. Neuron *93*, 747–765.

Sherin, J.E., Elmquist, J.K., Torrealba, F., and Saper, C.B. (1998). Innervation of histaminergic tuberomammillary neurons by GABAergic and galaninergic neurons in the ventrolateral preoptic nucleus of the rat. J. Neurosci. *18*, 4705–4721.

Taylor, N.E., Van Dort, C.J., Kenny, J.D., Pei, J., Guidera, J.A., Vlasov, K.Y., Lee, J.T., Boyden, E.S., Brown, E.N., and Solt, K. (2016). Optogenetic activation of dopamine neurons in the ventral tegmental area induces reanimation from general anesthesia. Proc. Natl. Acad. Sci. USA *113*, 12826–12831.

Trudel, E., and Bourque, C.W. (2010). Central clock excites vasopressin neurons by waking osmosensory afferents during late sleep. Nat. Neurosci. *13*, 467–474.

Tung, A., Szafran, M.J., Bluhm, B., and Mendelson, W.B. (2002). Sleep deprivation potentiates the onset and duration of loss of righting reflex induced by propofol and isoflurane. Anesthesiology *97*, 906–911.

Tung, A., Bergmann, B.M., Herrera, S., Cao, D., and Mendelson, W.B. (2004). Recovery from sleep deprivation occurs during propofol anesthesia. Anesthesiology *100*, 1419–1426.

Urade, Y., and Hayaishi, O. (2011). Prostaglandin D2 and sleep/wake regulation. Sleep Med. Rev. *15*, 411–418.

Van Dort, C.J., Zachs, D.P., Kenny, J.D., Zheng, S., Goldblum, R.R., Gelwan, N.A., Ramos, D.M., Nolan, M.A., Wang, K., Weng, F.J., et al. (2015). Optogenetic activation of cholinergic neurons in the PPT or LDT induces REM sleep. Proc. Natl. Acad. Sci. USA *112*, 584–589.

Watson, S.J., Akil, H., Fischli, W., Goldstein, A., Zimmerman, E., Nilaver, G., and van wimersma Griedanus, T.B. (1982). Dynorphin and vasopressin: common localization in magnocellular neurons. Science *216*, 85–87.

Weber, F., and Dan, Y. (2016). Circuit-based interrogation of sleep control. Nature *538*, 51–59.

Weber, F., Hoang Do, J.P., Chung, S., Beier, K.T., Bikov, M., Saffari Doost, M., and Dan, Y. (2018). Regulation of REM and non-REM sleep by periaqueductal GABAergic neurons. Nat. Commun. *9*, 354.

Weiss, M.L., and Cobbett, P. (1992). Intravenous injection of Evans Blue labels magnocellular neuroendocrine cells of the rat supraoptic nucleus in situ and after dissociation. Neuroscience *48*, 383–395.

Xie, L., Kang, H., Xu, Q., Chen, M.J., Liao, Y., Thiyagarajan, M., O'Donnell, J., Christensen, D.J., Nicholson, C., Iliff, J.J., et al. (2013). Sleep drives metabolite clearance from the adult brain. Science *342*, 373–377.

Yamashita, T., and Yamanaka, A. (2017). Lateral hypothalamic circuits for sleep-wake control. Curr. Opin. Neurobiol. *44*, 94–100.

Yizhar, O., Fenno, L.E., Davidson, T.J., Mogri, M., and Deisseroth, K. (2011). Optogenetics in neural systems. Neuron *71*, 9–34.

Yu, X., Ye, Z., Houston, C.M., Zecharia, A.Y., Ma, Y., Zhang, Z., Uygun, D.S., Parker, S., Vyssotski, A.L., Yustos, R., et al. (2015). Wakefulness is governed by GABA and histamine cotransmission. Neuron *87*, 164–178.

Zhang, Z., Ferretti, V., Güntan, İ., Moro, A., Steinberg, E.A., Ye, Z., Zecharia, A.Y., Yu, X., Vyssotski, A.L., Brickley, S.G., et al. (2015a). Neuronal ensembles sufficient for recovery sleep and the sedative actions of α2 adrenergic agonists. Nat. Neurosci. *18*, 553–561.

Zhang, Y., Zhao, S., Rodriguez, E., Takatoh, J., Han, B.X., Zhou, X., and Wang, F. (2015b). Identifying local and descending inputs for primary sensory neurons. J. Clin. Invest. *125*, 3782–3794.

Zimmerman, C.A., Leib, D.E., and Knight, Z.A. (2017). Neural circuits underlying thirst and fluid homeostasis. Nat. Rev. Neurosci. *18*, 459–469.

STAR★METHODS

KEY RESOURCES TABLE

REAGENT or RESOURCE	SOURCE	IDENTIFIER
Antibodies		
goat anti-Fos	Santa Cruz Biotechnology	Cat# sc-52-G; RRID: AB_2629503
donkey anti-goat Alexa Fluor 488	Jackson ImmunoResearch	Cat# 705-545-147; RRID: AB_2336933
Bacterial and Virus Strains		
CANE-LV-Cre	Sakurai et al., 2016	N/A
AAV8-hSyn-DIO-mCherry	Addgene	50459-AAV8
AAV8-hSyn-DIO-hM3D (Gq)-mCherry	Addgene	44361-AAV8
AAV1-CAG-DIO-GFP	UNC Vector Core	N/A
AAV1-Ef1a-DIO-hChR2(H134R)-eYFP	Addgene	20298-AAV1
AAV1-Ef1a-DIO-eArch3.0-eYFP	UNC Vector Core	N/A
AAV8-hSyn-DIO-DTR	Boston Children's Hospital Viral Core	N/A
Chemicals, Peptides, and Recombinant Proteins		
Isoflurane	Baxter Health Corporation	NDC 10019-360-60
Ketamine	Henry Schein	NDC 11695-6835-1
xylazine	Akorn, Inc	NDC 59399-111-50
Propofol	Sigma-Aldrich	D126608
Intralipid	Sigma-Aldrich	I141
Dexmedetomidine	Sigma-Aldrich	SML0956
Clozapine N-oxide (CNO)	Sigma-Aldrich	C0832
Diphtheria toxin (DT)	Sigma-Aldrich	D0564
Fluorogold	Fluorochrome	N/A
Experimental Models: Organisms/Strains		
wild type C57BL/6J mice	Jackson Laboratory	664
Fos^{TVA} knockin mice	Jackson Laboratory	027831
AVP-IRES2-Cre-D mice	Jackson Laboratory	23530
Oligonucleotides		
See Table S1 for the primers	N/A	N/A
Software and Algorithms		
MATLAB 2016a	MathWorks	RRID: SCR_001622
CerePlex Direct	BlackRock Microsystem	N/A
Offline Sorter	Plexon	RRID: SCR_000012
SIRENIA SLEEP PRO	Pinnacle Technology	N/A
Prism	GraphPad	RRID: SCR_002798
SPSS	IBM	RRID: SCR_002865
Spike2 software	Cambridge Electronic Design	RRID: SCR_000903
ImageJ	NIH Image	RRID: SCR_003070
ZEN	ZEISS	N/A
Other		
gas-tight syringe	New Era Pump Systems Inc	N/A

CONTACT FOR REAGENT AND RESOURCE SHARING

Further information and requests for resources and reagents should be directed to and will be fulfilled by the Lead Contact, Fan Wang (fan.wang@duke.edu).

EXPERIMENTAL MODEL AND SUBJECT DETAILS

Animals

Adult male Fos^{TVA} knockin mice (Sakurai et al., 2016) were used in this study (available from JAX stock #027831). Adult AVP-IRES-Cre (JAX stock #023530) and C57BL/6 mice were obtained from Jackson Laboratory. For chemogenetic activation of SON AVP neurons, adult male heterozygous $AVP^{Cre/+}$ mice were used. For labeling of AANs with CANE technology, adult Fos^{TVA} mice were single-house for two days to quench the background *c-fos* expression. Subjects were randomly assigned to experimental and control groups. Animals were housed in standard 12-h dark/12-h light cycle at common facility and all experimental procedures were approved by Duke Animal Care and Use Program.

METHOD DETAILS

Viral Vectors

The CANE-LV-Cre was generated as previously described (Sakurai et al., 2016). Cre-inducible AAV vectors AAV8-hSyn-DIO-hM3D (Gq)-mCherry and AAV8-hSyn-DIO-mCherry, AAV1-EF1a-DIO-hChR2 (H134R)-EYFP were purchased from Addgene. AAV1-CAG-DIO-GFP and AAV1-EF1a-DIO-eArch3.0-EYFP were purchased from the University of North Carolina (UNC) Vector Core. AAV8-hSyn-DIO-DTR was produced by the viral vector core of the Boston Children's Hospital.

Immunofluorescence

After acutely anesthetized with isoflurane, mice were transcardially perfused with PBS (pH7.4), followed by ice-cold 4% paraformaldehyde (PFA) in PBS. The dissected brains were further post-fixed overnight in 4% PFA at 4°C, and then transferred into 30% sucrose PBS buffer for 48 h. Later, the brains were frozen in Tissue-Tek O.C.T. Compound (Sakura) and sliced at 60 μm with cryostat (Leica Biosystems). The sections were washed with PBS, incubated with 1% Triton in PBS at room temperature for 1 h, and applied with blocking solution (10% Blocking One (nacalai tesque) in PBS with 0.3% Triton X-100) at room temperature for 1 h. Then, the sections were treated with appropriate primary antibodies with desired concentration in blocking solution at 4°C for overnight. After washed by PBS three times, the sections were incubated with secondary antibody at 4°C for another night. The sections were further washed, mounted, and coverslipped. The primary antibodies used in this study are: goat anti-Fos (Santa Cruz Biotechnology, sc52-g, 1:300). The secondary antibodies are: Alexa Fluor 488 donkey anti-goat (Jackson immunoresearch, 705-545-147 1:400).

Two-Color *in situ* Hybridization

The cDNA fragments of mouse *c-fos*, *vGlut2*, *vGat*, *prodynorphin*, and *oxytocin*, *vasopressin*, and *galanin* were amplified by PCR with the antisense primer incorporating the T7 promoter sequence. *In vitro* transcription was then performed based on the PCR-amplified template using T7 RNA polymerase with DIG-UTP (Roche) or fluorescein-UTP (Roche) for the synthesis of the antisense probes. After hybridization and washing as the protocols we previously described (Bellavance et al., 2017; Zhang et al., 2015b), sections were first incubated with alkaline phosphatase–conjugated anti-DIG (1:3500, Roche) and developed with Fast Red substrate (Sigma). Subsequently, the sections were further incubated with POD anti-FITC (1:500, Roche), and developed with FITC-TSA (PerkinElmer).

Capturing AANs Using CANE

Adult Fos^{TVA} (more than 8-week old) mice were single-house for two days to quench the background *c-fos* expression. On the third day, mice were first put under sustained GA (1%∼1.2% isoflurane) for 1.5 h, then a stereotaxic surgery was performed, CANE-LV-Cre (500-750 nl) mixed with desired virus (see below) were co-injected into unilateral or bilateral AAN target area (AP 0.0, ML ± 1, DV −5.30∼5.40 from the Bregma). For axon-tracing experiment, AAV1-CAG-DIO-GFP (300-500 nl) was co-injected; for AAN labeling and recording, either AAV8-hSyn-DIO-mCherry (500 nl) or AAV1-CAG-DIO-GFP (500 nl) was co-injected; for chemogenetic activation or control experiments, AAV8-hSyn-DIO-hM3D (Gq)-mCherry (500 nl) or AAV8-hSyn-DIO-mCherry (500 nl) was co-injected; for optogenetic activation and inhibition, AAV1-EF1a-DIO-hChR2 (H134R)-EYFP and AAV1-EF1a-DIO-eArch3.0-EYFP were co-injected; for AAN ablation, AAV8-hSyn-DIO-DTR (500 nl) was co-injected. ParaSON is defined as a brain region located within 500 μm radius circle with the up-corner of the optic chiasm or tract as the center, extending from anterior to posterior hypothalamus.

Labeling of Neuroendocrine Cells with Peripheral Fluorogold Injection

To identify neuroendocrine cells, we adapt the protocol as previous described (Kriegsfeld et al., 2003; Oyola et al., 2017). Briefly, mice were injected subcutaneously with 50 μL of 5% Fluorogold (Fluorochrome, Denver, Colorado) in saline. Five to six days later, animals were transcardially perfused with PBS, followed by 4% PFA. The brains were further removed, postfixed overnight, sectioned at 60 μm with cryostat, and the images were taken with Zeiss 700 laser scanning confocal microscopy.

Axon-Tracing and Quantification

CANE-LV-Cre (500 nl) and AAV1-CAG-DIO-GFP (300-500 nl) were co-injected into AAN region of adult Fos^{TVA} mice. After the viral constructs fully expressed, mice were then sacrificed, the brain were cut into serial 80 μm sections with cryostat (Leica Biosystems). The images were taken with Zeiss 700 laser scanning confocal microscopy. We adopted a similar strategy used by Allen Brain

Institute to quantify AAN projection (Oh et al., 2014). In brief, GFP intensity were first normalized and binarized with a custom-written MATLAB code. Region of interests (ROI) were manually defined with respect to standard atlas. GFP positive pixels and total number of pixels in each ROI were quantified.

Multi-channel *In Vivo* Recording and Data Analysis

Custom-built microelectrode array with 3∼4 electrode bundles (30 μm diameter tungsten, California Fine Wire) and two EMG wires (Stablohm 650, California Fine Wire) were constructed as previously described. One wire bundle (with 9 wires) were placed into AAN region (AP: 0.0, ML: ± 1.00, DV: −5.40∼5.50) to record the single-unit activity. Another bundle (with 6 wires) were placed into frontal cortex (AP: 1.70, ML: ± 0.30, DV: −2.00) to capture brain oscillations. EMG wires were inserted into neck muscles. Mice were allowed to recover at least ten days before experiments. For each experimental session, mice were placed in the recording chamber connected with standard Isoflurane vaporizer. After initial 5 min of baseline recording (continuously infused with oxygen), isoflurane (1%∼1.2%) was applied into the chamber for 10 min, then the mice were allowed to emerge from GA for another 20 min. Neuronal spikes, local field potential, and muscle activity were recorded with CerePlex Direct (BlackRock Microsystem). Brain states were determined by frontal cortex neural oscillations and EMG activity. Spike-sorting were manually done with Offline Sorter (Plexon) based on principal component analysis (PCA). Single-units were identified with distinct clusters (nicely separated from other units and noise) in PCA space and shown clear refractory period in autocorrelation histograms.

Units were classified into three categories based on the responsive property toward isoflurane exposure. Since the mice typically lose consciousness around 400 s (100 s after 1%∼1.2% Isoflurane infusion) and wake up around 1000∼1400 s (100∼500 s after Isoflurane withdraw) with 10 min total duration of isoflurane exposure, we calculated average spike rate for each unit during 400∼1200 s and compared with baseline spike rate of wakefulness 0∼400 s. Units with mean spike rate increase more than double (> 2) were identified as isoflurane-activated cells, while units with mean spike rate decrease more than a half (< 1/2) were classified as isoflurane-suppressed cells. The rest were weak-modulated cells. For illustration purpose, the spike rate of each unit was smoothed with Gaussian kernel and normalized with peak firing rate. To capture the neuronal dynamics across brain state transitions (LOC and Emergence), spike density function (SDF) for each neuron is built by convolving Gaussian kernels (1 s-length for main Figure 1 and 0.3 s- and 3 s-length for Figure S2) with raw spike train.

Slice Electrophysiology

Coronal slices of hypothalamus were prepared from the adult male AAN-mCherry mice. Animals were briefly anesthetized with 1.2% isoflurane and then killed by decapitation, and brain tissues were immediately dissected out and immersed in ice-cold oxygenated (95% O2 and 5% CO2) slicing solution in which isotonic sucrose was used as a substitute for NaCl (2.5 KCl, 1.25 NaH2PO4, 25 NaHCO3, 7 MgCl2, 0.5 CaCl2, 7 dextrose, 210 sucrose, 3 sodium pyruvate, 1.3 ascorbic acid). Slices (250 μm in thickness) were cut with a Leica microtome (VT-1000s, Leica, Germany) and immediately transferred to an incubation beaker filled with aerated holding solution: 125 NaCl, 2.5 KCl, 1.25 NaH2PO4, 25 NaHCO3, 2 MgCl2, 2 CaCl2, 12.5 dextrose, 3 sodium pyruvate, 1.3 ascorbic acid. After about 60-min incubation, we transferred slices to a submerged chamber perfused with aerated normal ACSF containing (in mM): 124 NaCl, 2.5 KCl, 1.25 NaH2PO4, 26 NaHCO3, 2 MgSO4, 2.5 CaCl2, 10 dextrose (315 mOsm, pH 7.4) and visualized by infrared differential interference contrast and fluorescence video microscopy (Examiner.D1, Zeiss). The patch-clamp electrode (4–6 MΩ) was filled with an intracellular solution containing 130 K-gluconate, 5 NaCl, 10 phosphocreatine disodium salt, 1 MgCl2, 10 HEPES, 0.02 EGTA, 0.5 Na2GTP, 2 MgATP, and 0.1% biocytin (pH 7.3, 280-290 mOsm). We employed a MultiClamp 700B amplifier (Molecular Devices) for patch-clamp recording and Spike2 software (Cambridge Electronic Design) for data acquisition. Non-volatile drugs propofol (15 μM, D126608, sigma), Ketamine (100 μM, Henry Schein), dexmedetomidine hydrochloride (40 μM, SML0956, sigma) and CNO (10 μM, Sigma-Aldrich C0832) were diluted from stock in fresh oxygenated aCSF immediately prior to use. Volatile drugs, isoflurane (25 μl) was sonicated into solution in preoxygenated aCSF (50 mL), then stored in a gas-tight syringe (New Era Pump Systems) to prevent evaporation.

Drug Administration

For chemogenetic activation in freely behaving mice, Clozapine N-oxide (CNO, Sigma-Aldrich C0832) was dissolved in 0.2 mL vehicle solution (PBS with 0.3% DMSO) and administered intraperitoneally (3 mg per kg). Ketamine (100 mg per kg) with or without xylazine (10 mg per kg) were dissolved in PBS and injected intraperitoneally. Dexmedetomidine (Sigma-Aldrich, SML0956) was dissolved in PBS injected intraperitoneally (100 μg per kg). Propofol (Sigma-Aldrich, D126608) was dissolved in intra-lipid solution (I141, sigma) injected intraperitoneally (180 mg per kg). Diphtheria toxin (DT, Sigma-Aldrich, D0564) was dissolved in PBS and intraperitoneally injected (50 μg per kg).

EEG and EMG Recording and Analysis

After the recovery from virus injection surgery (3-4 weeks), mice were further implanted with EEG and EMG. For chemogenetic activation experiment, three stainless steel screws were placed on the frontal, parietal, and cerebellar cortex as EEG electrodes and two thin microwires (Stablohm 650, California Fine Wire) were inserted into bilateral neck muscles as EMG electrodes. For optogenetic activation, two optic fibers (200 μm, NA, 0.39, Thorlab) were inserted on top of AAN (AP 0.0 ∼-0.3, ML ± 1, DV −5.00 ∼5.20 from the Bregma) two stainless steel screws were placed on the parietal cortex and cerebellum, and EMG were inserted into neck muscles.

Both EEG and EMG were connected into Omnetics connectors and recorded with CerePlex Direct (BlackRock Microsystem) at 2000 Hz. For chemogenetic activation experiments, after habituation to the recording chambers (Med Associates), experimental sessions typically began at 21:00 (dark phase) after either vehicle or CNO injections. For optogenetic experiment, after habituation to the recording chamber, experiments were performed from 20:30 to 24:00. Two laser trains (10 Hz, 10 ms, 1 s-ON and 1 s-OFF, 3 min, 3∼4 mW from the fiber tip, 473-nm Blue Laser, Cobolt, Sweden) were given per experimental trial with inter-trial interval of 1∼1.5 h. Each animal was tested for 2∼3 experimental trials (4∼6 pulse trains). Brain state was semi-automatically scored at 4 s epochs with custom-written MATLAB code (MathWorks) by the researchers blinded to experimental treatments. Slow-wave sleep was defined as high delta (1-4 Hz) power in the EEG and low EMG activity; REM sleep was defined as high theta (6-10 Hz) power in the EEG with minimal EMG signals; wakefulness was identified as small amplitude and high-frequency EEG with tonic EMG activity. Spectrograms were generated with multi-taper approach (Prerau et al., 2017). EEG power spectra were computed for consecutive 4 s windows within the frequency range of 0-50 Hz using the Fast Fourier Transform (FFT). The frequency resolution was set at 0.25 Hz and the power of interested frequency was further divided by the total power.

For optogenetic activation experiments during general anesthesia, mice were first habituated to the recording chamber. Later, one train of laser pulse (10 Hz, 10 ms, 1 s-ON and 1 s-OFF, 3 min, 3∼4 mW from the fiber tip) was given to the animals followed by 1% Isoflurane anesthesia for 12 min. For optogenetic inhibition experiments, yellow laser light (5-min square pulse, 5∼7 mW measured at the fiber tip, 561-nm DPSS Laser, OptoEngine LLC, Utah) was delivered for the first 5 min of Isoflurane anesthesia (1% isoflurane for 10 min). The time of Induction was determined by the onset of strong slow-wave power in EEG and minimal muscle activity in EMG; the time point of Fully Awake was determined by diminished slow-wave power and re-appearance of movement continuously for at least 1 min; the total Duration of unconscious time was calculated by the time point of Fully Awake minus the time point of Induction.

For DT/DTR ablation experiment, commercially available EEG and EMG headmounts (Pinnacle Technology, #8201-SS) were used. The electrical signals were acquired at 1000 Hz with EEG and EMG system from Pinnacle Technology. After habituation to the recording chamber, experiments were typically begun at 19:00 and continued toward 18:00 on the next day (23 h of continuous recordings). Brain states were scored at 10 s epochs by the researchers blinded to experimental treatments with software SIRENIA SLEEP PRO (Pinnacle Technology). For EEG power bands analysis, the delta (1-4 Hz) power of SWS and the theta (6-10 Hz) power of REM sleep are computed with FFT. For each mouse, the median values of power across all the corresponding windows are used for further statistical analysis.

Mild Sleep Deprivation and Recovery

Mice were kept in their home cages with freely access to water and foods. Sleep deprivation typically began at the light phase from 9:00 to 14:00. Mice were kept awake by introducing novel objects, cage tapping, and rotation every 30 min. Recovery sleep was allowed from 14:00 to 17:00. At the end of behavior sessions, Fos staining were performed as described above.

QUANTIFICATION AND STATISTICAL ANALYSIS

For paired observations in slice electrophysiology experiment, Wilcoxon signed-rank test was used to examine the difference between groups. For chemogenetic experiments, mice were randomly assigned to saline or CNO injection in counterbalance order, two-way repeated-measured ANOVA followed by Sidak's post hoc test (AAN-hM3Dq experiment) or paired t test (AVP-hM3Dq) was used to assess the statistical difference. For optogenetic experiment, permutation tests (> 10000 iterations) were performed between AAN-ChR2 and AAN-GFP groups across SWS, Wake, REM. For general anesthesia induction experiment, two-sample t test was used to compare AAN-GFP and AAN-ChR2 groups, or to compare AAN-GFP and AAN-eArch3.0 groups. For DTR-ablation experiment, one-way repeated-measures ANOVA followed by Sidak's post hoc test was used. Statistical analysis was conducted with Prism (GraphPad), SPSS (IBM) and MATLAB (MathWorks). All data were presented as mean ± SEM. Error bars in figures also represent SEM. In addition, the power spectra of SWS and Wake were also plotted with 95% confidence interval in Figure S5. Indications of significance level are as follows: *$p < 0.05$; **$p < 0.01$, and ***$p < 0.001$.

DATA AND SOFTWARE AVAILABILITY

Source data and MATLAB codes are available upon reasonable request.

Neuron, Volume *102*

Supplemental Information

A Common Neuroendocrine Substrate for Diverse General Anesthetics and Sleep

Li-Feng Jiang-Xie, Luping Yin, Shengli Zhao, Vincent Prevosto, Bao-Xia Han, Kafui Dzirasa, and Fan Wang

Supplemental Information

A Common Neuroendocrine Substrate for Diverse General Anesthetics and Sleep

Li-Feng Jiang-Xie, Luping Yin, Shengli Zhao, Vincent Prevosto, Bao-Xia Han, Kafui Dzirasa, Fan Wang

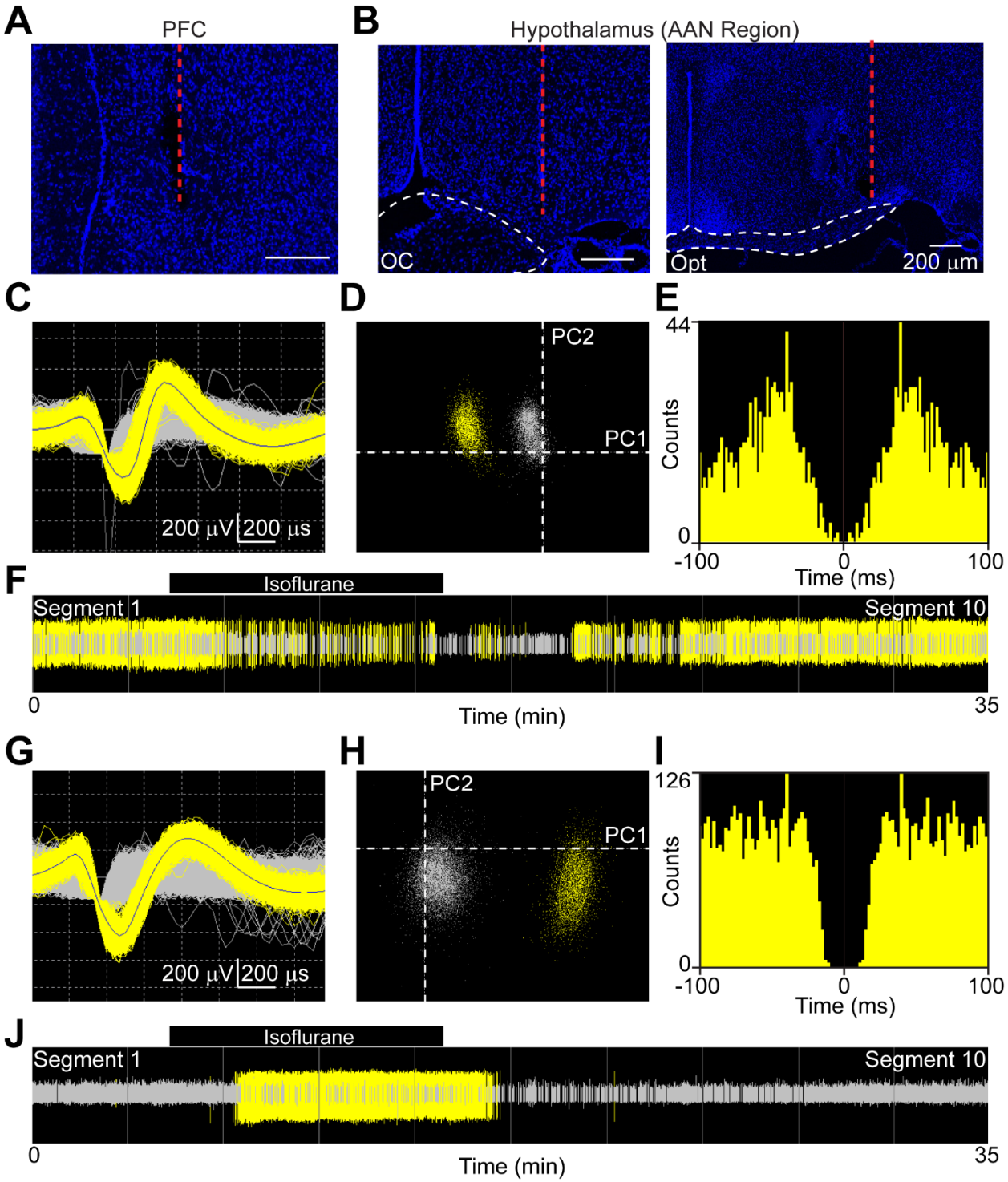
A
PFC
B
Hypothalamus (AAN Region)
OC
Opt
200 µm
C
200 µV
200 µs
D
PC2
PC1
E
44
Counts
0
-100
0
100
Time (ms)
F
Isoflurane
Segment 1
Segment 10
0
Time (min)
35
G
200 µV
200 µs
H
PC2
PC1
I
126
Counts
0
-100
0
100
Time (ms)
J
Isoflurane
Segment 1
Segment 10
0
Time (min)
35

Figure S1. Microwire electrode placement and examples of well-isolated single-unit AAN activity with Plexon Offline Sorter. Related to Figure 1.

(A-B) Example of electrode track (Red dashed line) in frontal cortex and the AAN region. **(C-F)** An example of isoflurane-suppressed neuron. (**G-J)** an example of isoflurane-activated neuron. Yellow, isolated unit; Gray, noise. **(C), (G)** Waveforms. **(D)**, **(H)** Cluster view in principle component space. PC1, principle component 1; PC2, principle component 2. **(E), (I)** Autocorrelogram. **(F), (J)** Identified spikes across recording session.

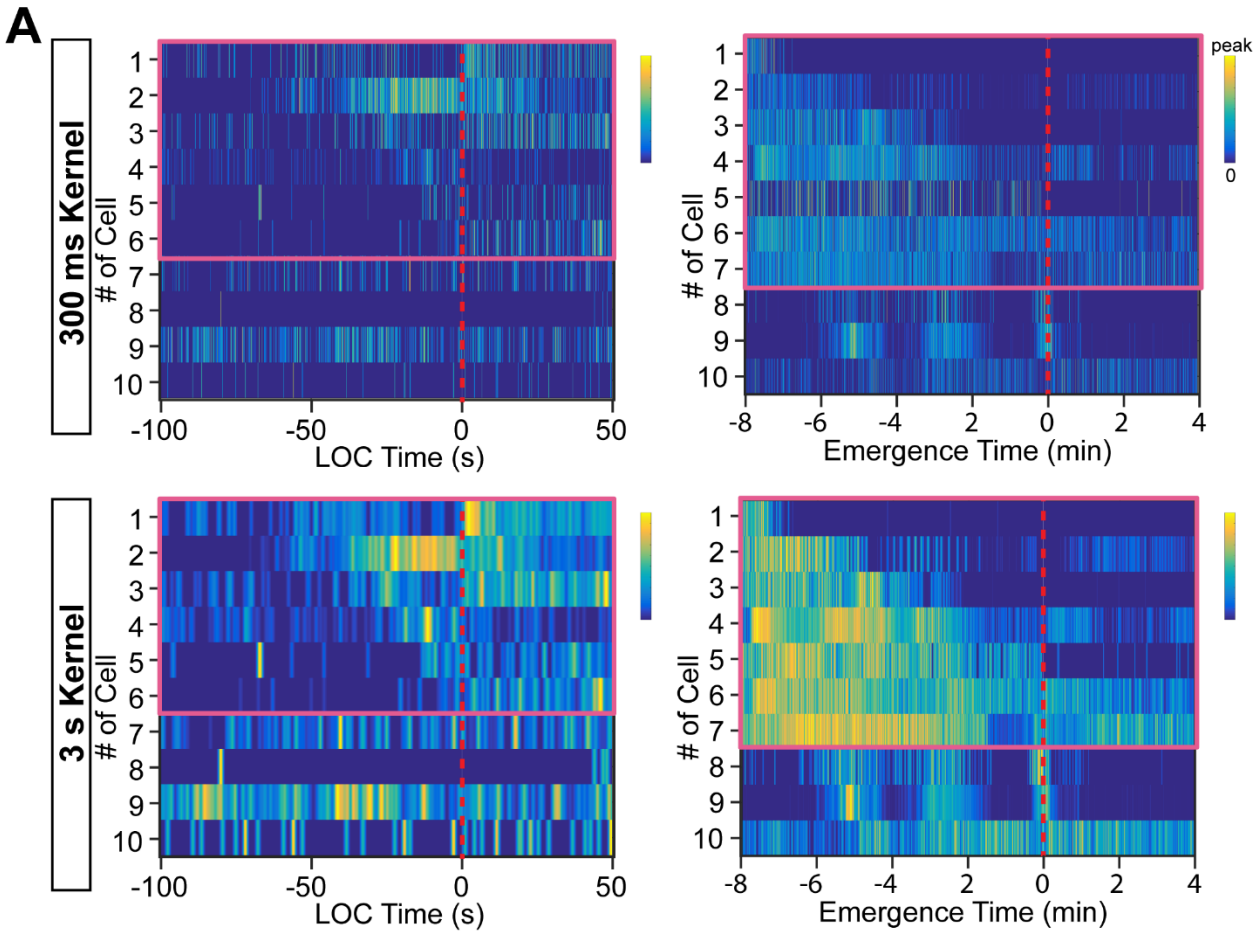

Figure S2. Activities of isoflurane-activated neurons estimated with different size of Gaussian kernels aligned with LOC and Emergence. Related to Figure 1.

(A) Top, 300-ms kernel; bottom, 3-s kernel. LOC, loss of consciousness.

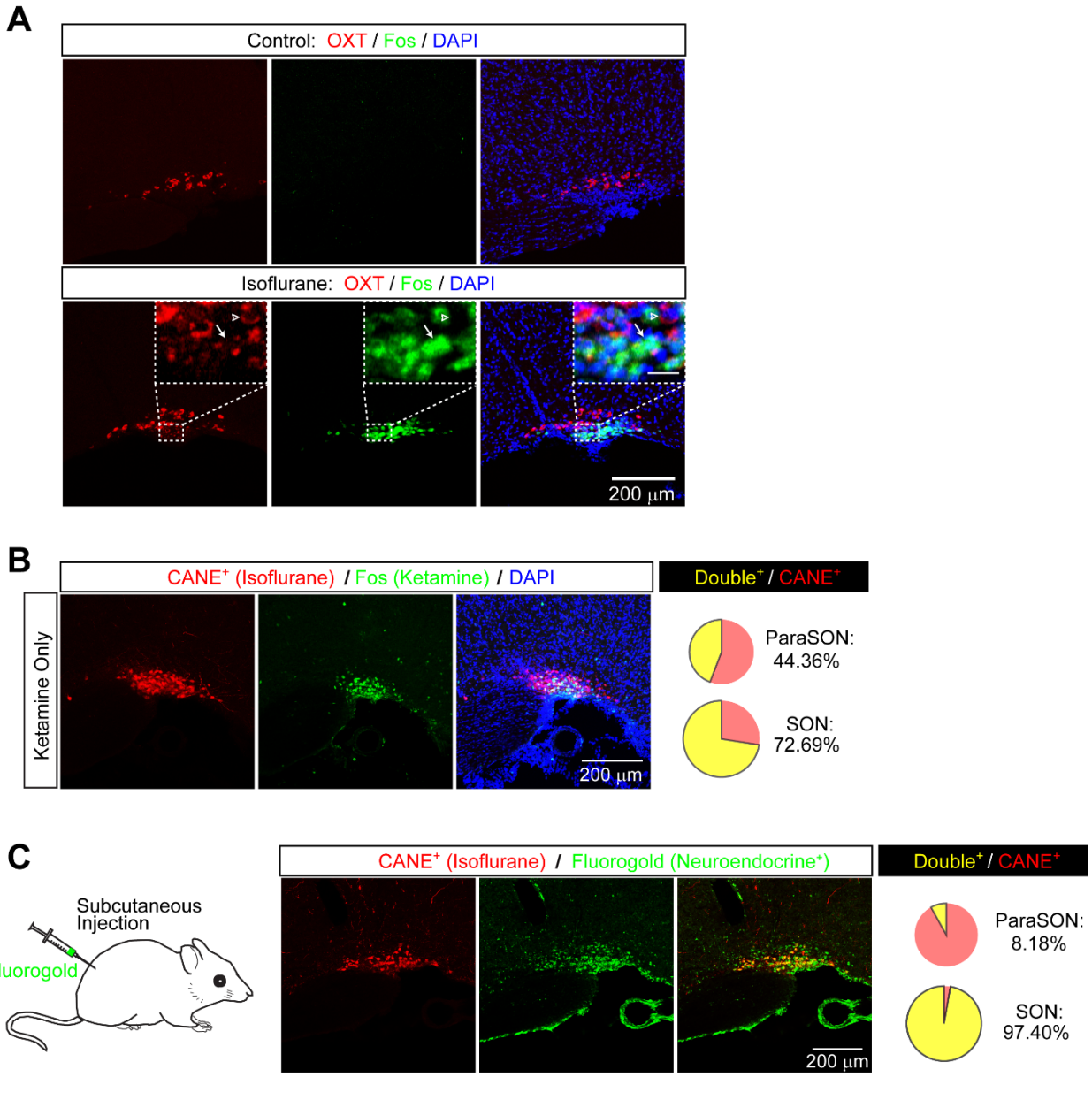
A
Control: OXT / Fos / DAPI
Isoflurane: OXT / Fos / DAPI
200 μm
B
CANE+ (Isoflurane) / Fos (Ketamine) / DAPI
Double+ / CANE+
Ketamine Only
200 μm
ParaSON:
44.36%
SON:
72.69%
C
Subcutaneous
Injection
Fluorogold
CANE+ (Isoflurane) / Fluorogold (Neuroendocrine+)
Double+ / CANE+
200 μm
ParaSON:
8.18%
SON:
97.40%

Figure S3. Extra molecular and histological characterization of AAN. Related to Figure 2 and 3.

(A) Isoflurane anesthesia induces dim oxytocin mRNA expression in SON. Top, unanesthetized (home cage) control; bottom, isoflurane anesthesia. Green, Fos; red: OXT, oxytocin; blue, DAPI. Arrow, open arrowhead indicating double$^+$ and OXT$^+$-only cells, respectively.

(B) Ketamine alone also induce Fos expression in AAN. Left panels, representative images of CANE-captured isoflurane-activated neurons (red) and Fos$^+$ neurons (green) induced by Ketamine treatment only. Right panels, pie charts showing the percentage of initial CANE-captured isoflurane-activated neurons that are re-activated (Fos$^+$) by Ketamine. 7-21 slices for each region from 2 mice.

(C) Hypothalamic AAN are neuroendocrine cells. Left, 5% Fluorogold (pseudocolor as green) was subcutaneously injected into AAN-mCherry mouse. Five days later, Fluorogold would be fully up-taken by neuroendocrine cells through the general circulation. Middle, representative colocalization image of AAN (mCherry) and neuroendocrine cells (green). Right, percentage of AAN colocalized with Fluorogold$^+$ cells. 15-25 slices for each region from 2 animals.

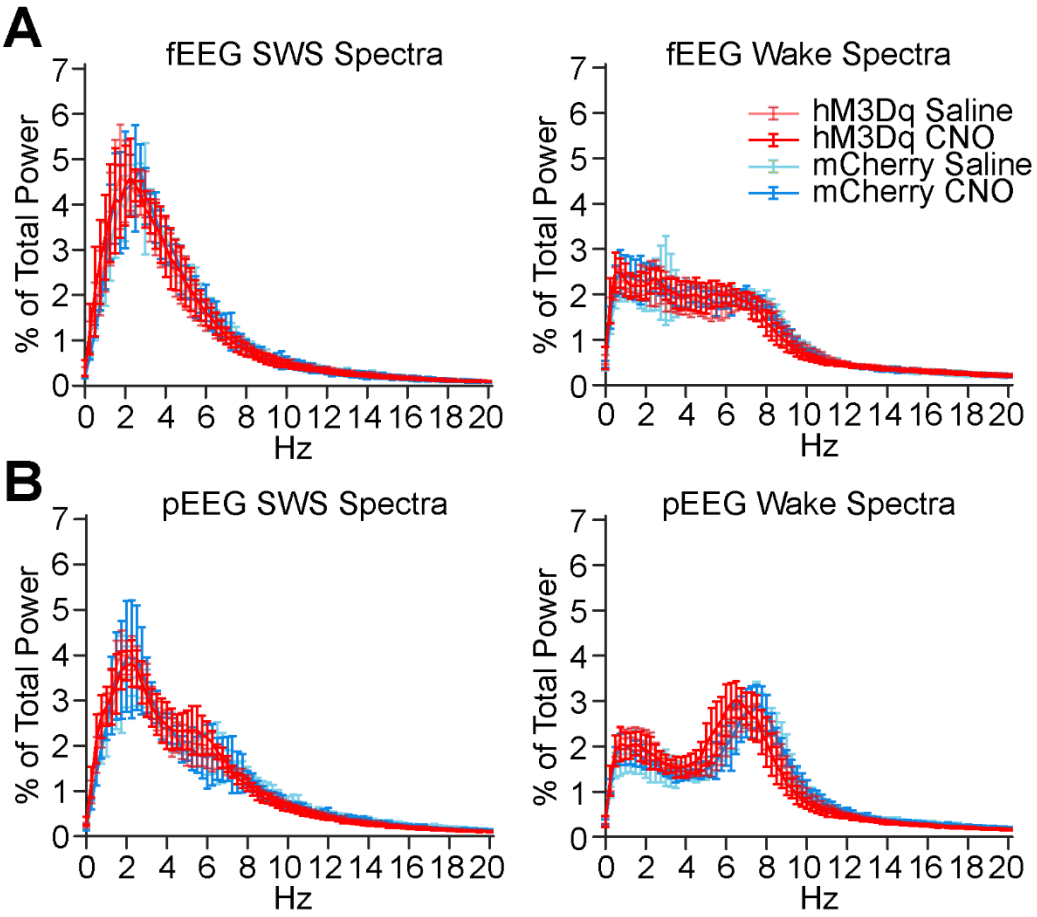

Figure S4. Power spectra of SWS and Wake plotted with 95% confidence interval (CI). Related to Figure 4.

(A-B) Power-frequency analysis of frontal **(A)** and parietal **(B)** EEG during SWS and Wake states for hM3Dq and mCherry groups following either saline or CNO treatment. fEEG, frontal EEG; pEEG, parietal EEG. *n* = 7 mice for hM3Dq and *n* = 4 mice for mCherry group.

Data are presented as mean ± 95% CI

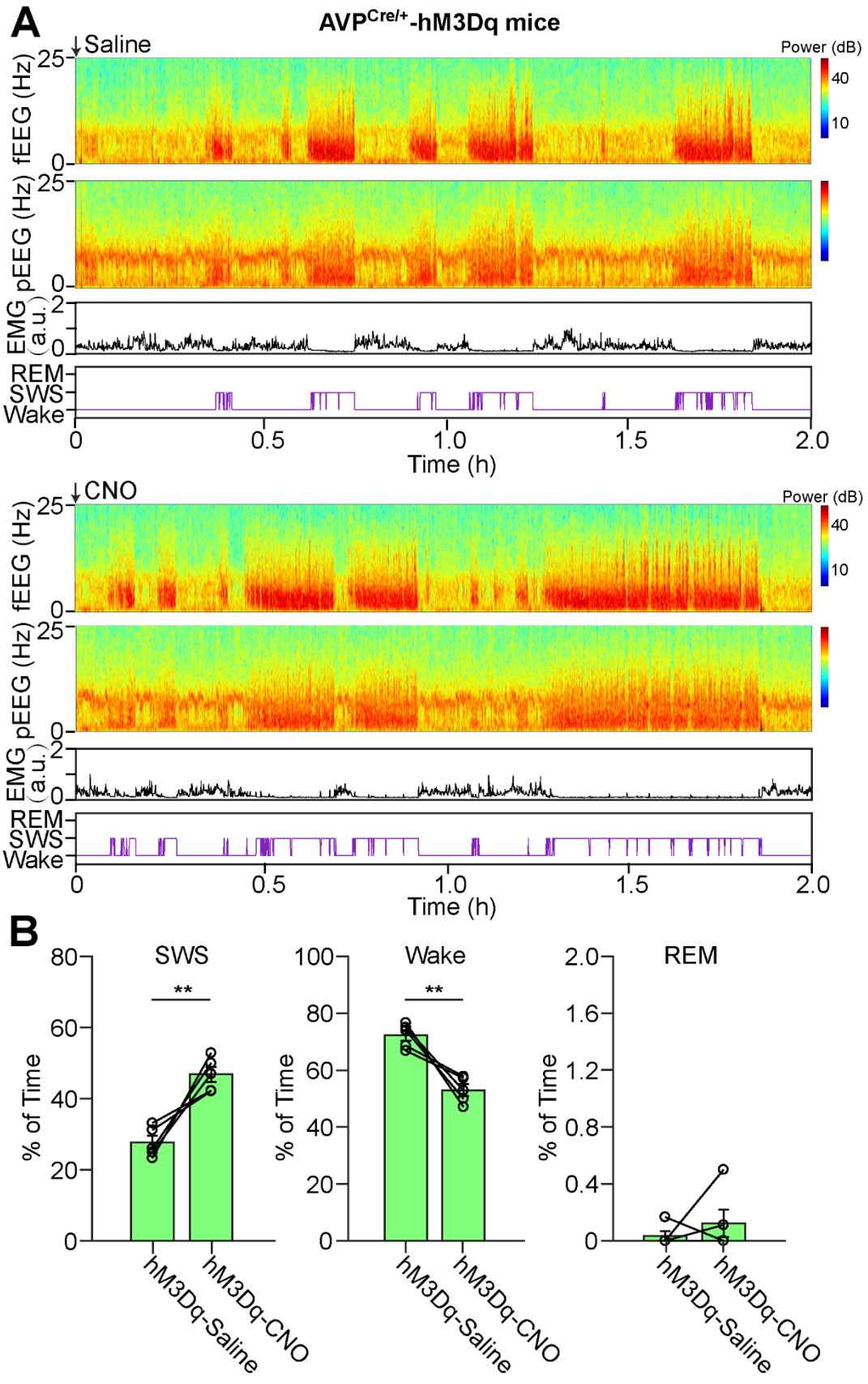
A
AVPCre/+-hM3Dq mice
Saline
Power (dB)
40
10
fEEG (Hz)
pEEG (Hz)
EMG (a.u.)
REM
SWS
Wake
Time (h)
CNO
B
SWS
Wake
REM
% of Time
**
hM3Dq-Saline
hM3Dq-CNO

Figure S5. Chemogenetic activation of SON AVP neurons potentiate SWS sleep. Related to Figure 4.

(A) Representative EEG/EMG recording following either saline (top) or CNO (bottom) injection. **(B)** Percentage of time spent on SWS, Wake and REM across 2 hours after saline or CNO injection. *n* = 5 mice. Paired-t test.

Data are presented as mean ± s.e.m., $^{**}P < 0.01$.

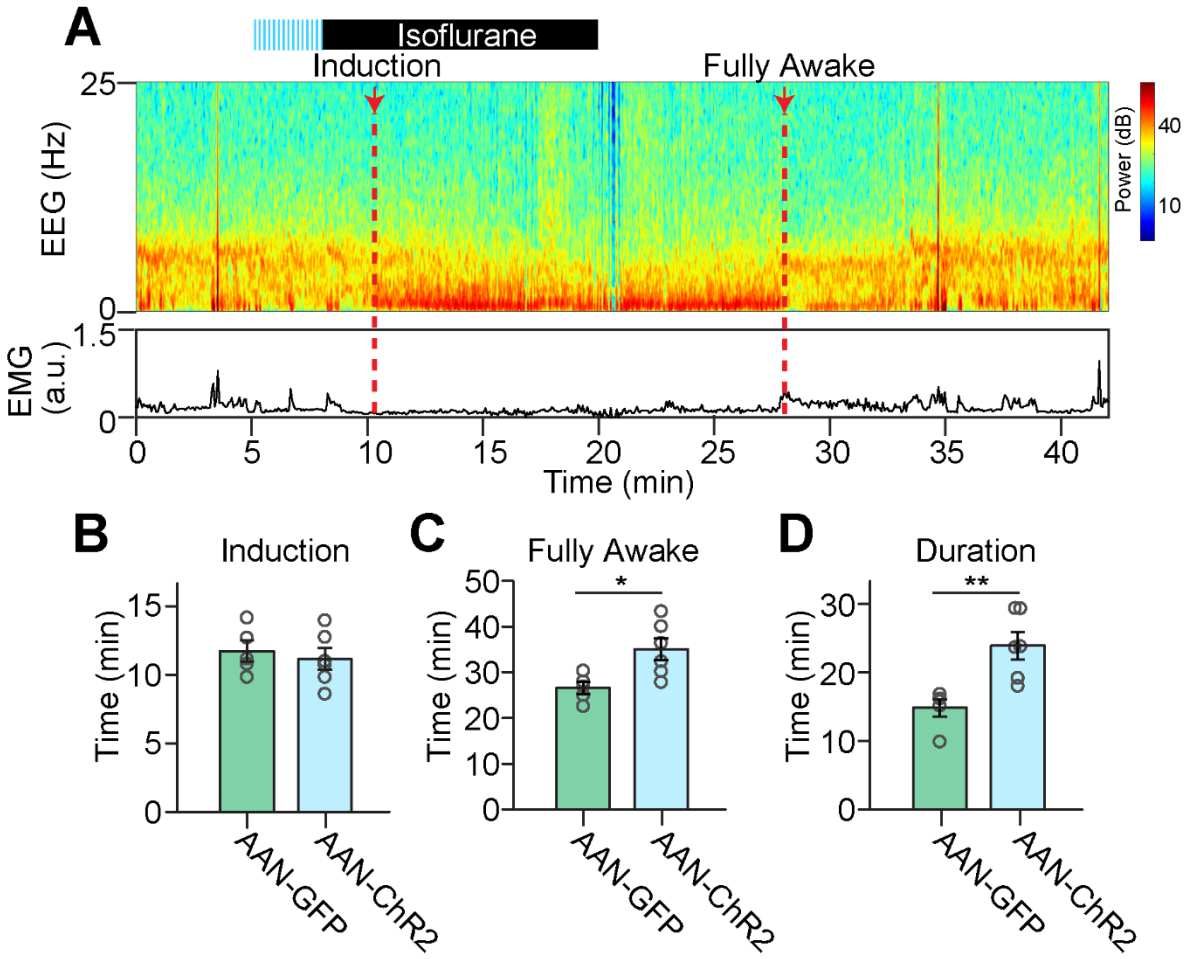

Figure S6. Optogenetic Activation of AAN Prolongs the Duration of GA. Related to Figure 5.

(A) Representative EEG/EMG recording across experimental session. Top, representative spectrogram of EEG; bottom, EMG. Isoflurane (1%) was infused immediately after laser stimulation (10 Hz, 10 ms pulses, 1s-On and 1s-OFF, 3 min, 3~4 mW measured at the fiber tips). Induction time is determined by appearance of slow oscillation and reduction of movement. Fully awake time is determined by reduction in slow-wave power and elevated muscle activity continuously for more than 1 min.

(B-D) Statistical analysis of Induction time **(B)**, fully awake time **(C)**, and anesthesia duration **(D)**. *n* = 5 for AAN-GFP mice, *n* = 6 for AAN-ChR2 mice. Two-sample t-test.

Data are presented as mean ± s.e.m., $^{*}P < 0.05$. $^{**}P < 0.01$.

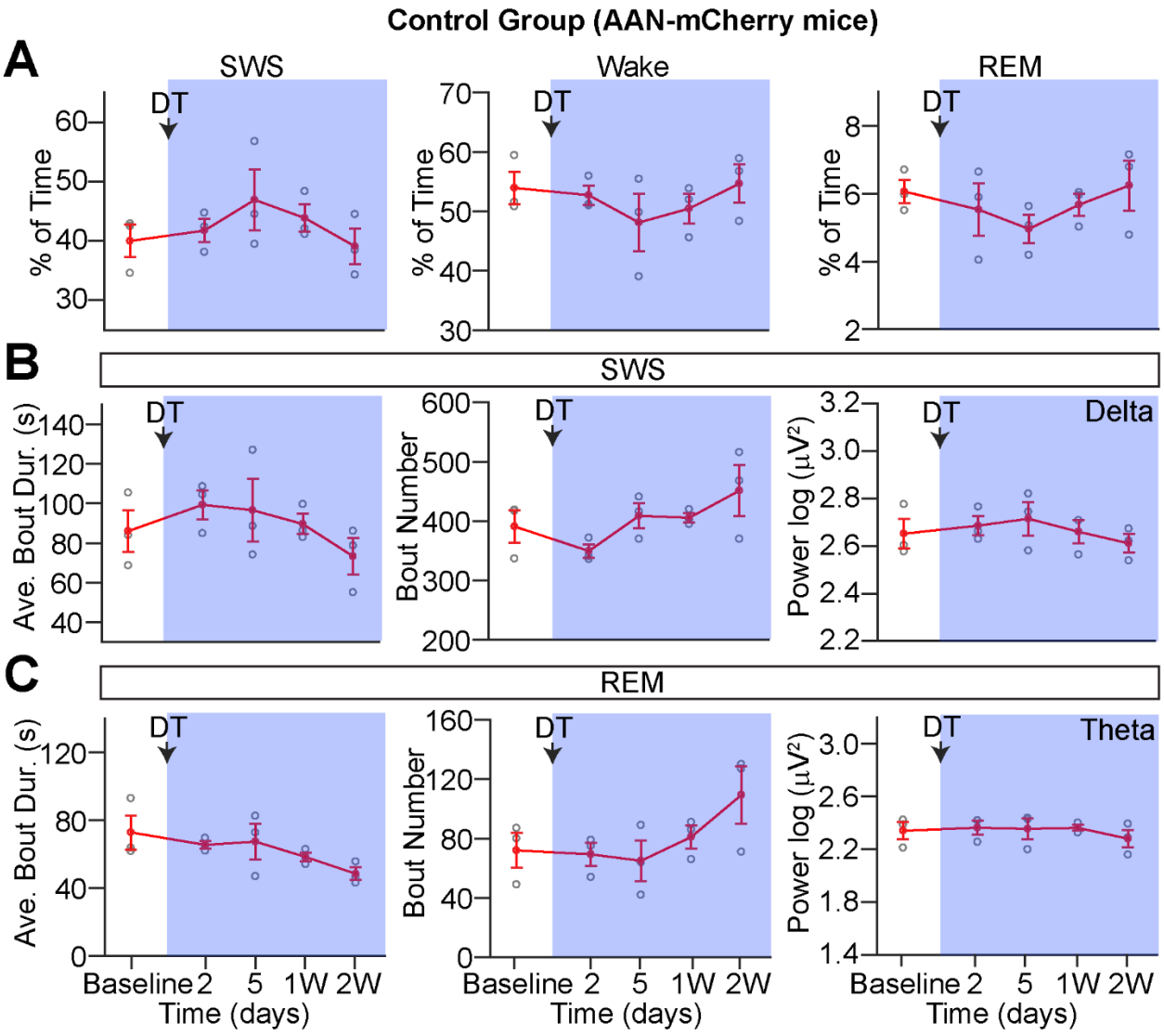

Figure S7. Diphtheria toxin (DT) in control AAN-mCherry mice. Related to Figure 7.

(A) Total percentage of time in SWS (left), Wake (middle), and REM sleep (right).

(B) Average bout duration, bout numbers, and delta power of SWS.

(C) Average bout duration, bout number, and theta power of REM. One-way repeated measures ANOVA followed by Sidak's post hoc test. *n* = 3 mice.

Data are presented as mean ± s.e.m.

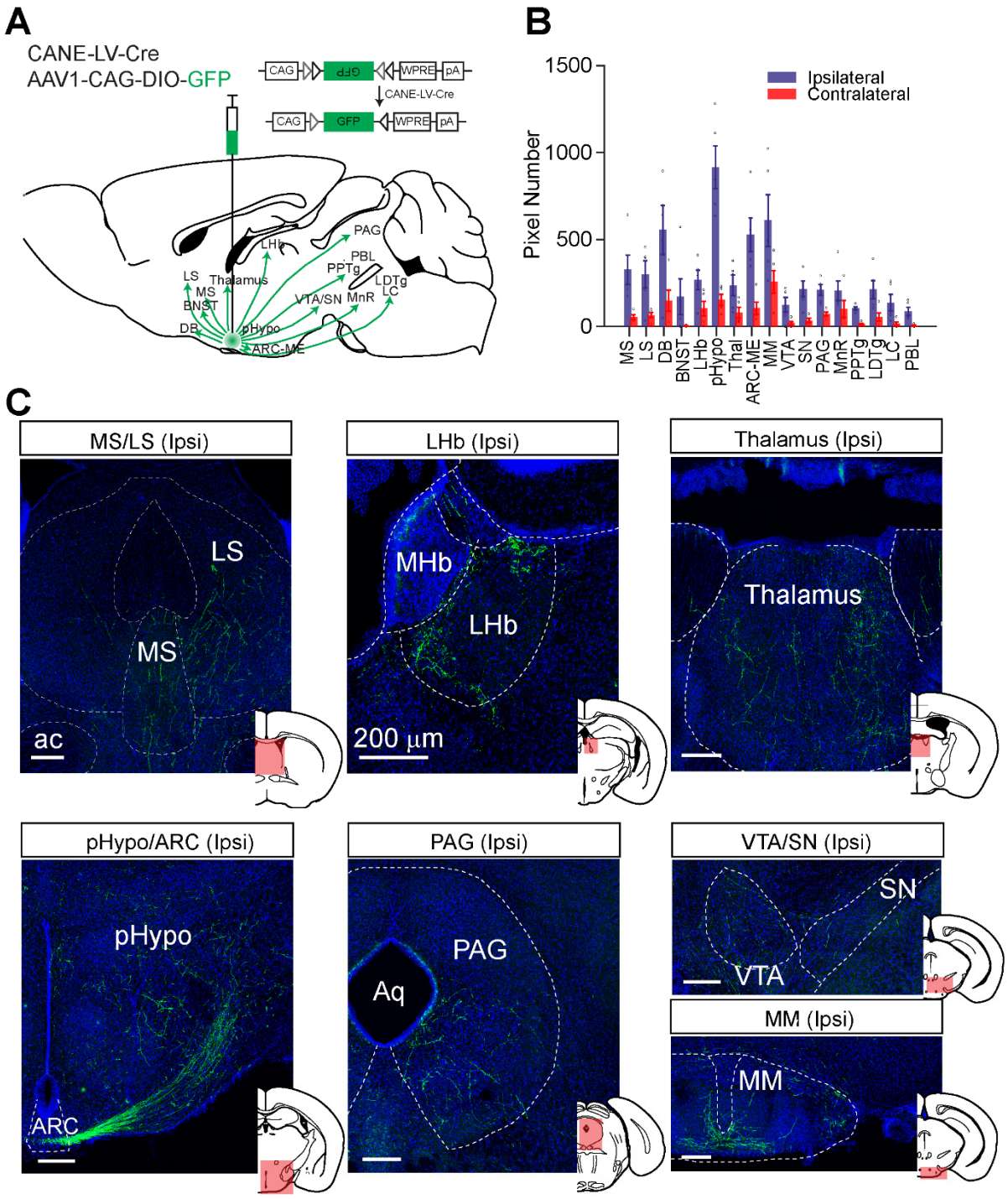
A
CANE-LV-Cre
AAV1-CAG-DIO-GFP
CAG
GFP
WPRE
pA
CANE-LV-Cre
LS
MS
BNST
Thalamus
LHb
PAG
PBL
PPTg
LDTg
LC
VTA/SN
MnR
DB
pHypo
ARC-ME
B
Ipsilateral
Contralateral
Pixel Number
1500
1000
500
0
MS
LS
DB
BNST
LHb
pHypo
Thal
ARC-ME
MM
VTA
SN
PAG
MnR
PPTg
LDTg
LC
PBL
C
MS/LS (Ipsi)
LS
MS
ac
LHb (Ipsi)
MHb
LHb
200 μm
Thalamus (Ipsi)
Thalamus
pHypo/ARC (Ipsi)
pHypo
ARC
PAG (Ipsi)
PAG
Aq
VTA/SN (Ipsi)
SN
VTA
MM (Ipsi)
MM

Figure S8. Projection Targets of AAN. Related to STAR Methods.

(A-B) Schematic summary of projection targets and quantification of projection densities of AAN. MS, medial septum; LS, lateral septum; DB, diagonal band of Broca; BNST, bed nucleus of the stria terminalis; LHb, lateral habenula; pHypo, posterior hypothalamus; Thal, thalamus; ARC-ME, arcuate nucleus-median eminence; MM, mammillary nucleus; VTA, ventral tegmental area; SN, substantia nigra; PAG, periaqueductal gray; MnR, median raphe nucleus; PPTg, pedunculopontine nucleus; LDTg, laterodorsal tegmental nucleus; LC, locus coeruleus; PBL, lateral parabrachial nucleus. *n* = 5 mice. Data are presented as mean ± s.e.m. **(C)** Representative images of projection targets. The shaded areas in the atlas indicate brain regions of interest. Green, AAN axon; Blue, DAPI.

Table S1. Primers for *in situ* Hybridization. Related to STAR Methods.

Primer	Sequence	SOURCE	IDENTIFIER
c-fos	*F*: AGAATCCGAAGGGAACGG	Allan Brain Atlas	Fos-RP_080109_01_B10
	R: GGAGGCCAGATGTGGATG		
vGlut2	*F*: CAAGAAGGTGCGCAAGACGCGTACACC	Bellavance et al., 2017	N/A
	R: TGCCCAAGCATTTCACAAAACACTGC		
vGat	*F*: GGCCACCTCCGTGTCCAACAAGTCC	Bellavance et al., 2017	N/A
	R: GAATTCGCTGGGCTGCTGCATGTTG		
Vasopressin (AVP)	*F*: CCGAGTGCCACGACGGTTT	Allan Brain Atlas	Avp-RP_070129_04_B12
	R: TTCCATGCTGTAGGGGCGAG		
Prodynorphin (Pdyn)	*F*: AGGAAAAGTTCAGGGGTCTCTC	Allan Brain Atlas	Pdyn-RP_050505_04_B03
	R: TCTCACAGTTCCCATGCAATAC		
Oxytocin (OXT)	*F*: CACCTACAGCGGATCTCAGAC	This paper	N/A
	R: AGACACTTGCGCATATCCAGG		
Galanin	*F*: ATCCTGCACTGACCAGCC	Allan Brain Atlas	Gal-RP_050303_02_F03
	R: TTGGCTTGAGGAGTTGGC		